2013

Analytical evaluation of mixing efficiencies and nonlinear interactions of turbulence in a stratified flow

Jennifer Lynn Jefferson
Iowa State University

Analytical evaluation of mixing efficiencies and nonlinear interactions of turbulence in a stratified flow

by

Jennifer Lynn Jefferson

A thesis submitted to the graduate faculty
in partial fulfillment of the requirements for the degree of
MASTER OF SCIENCE

Major: Civil Engineering (Environmental Engineering)

Program of Study Committee:
Chris Rehmann, Major Professor
Roy Gu
Hui Hu

Iowa State University
Ames, Iowa
2013

This thesis is dedicated to my greatest supporters – my husband, Jesse, my mom, Joyce, and my dad, David.

TABLE OF CONTENTS

LIST OF FIGURES

NOMENCLATURE

Roman symbols

a	$Gr^{-1}\kappa^2$, parameter used in solution for two active scalar case
a_S	$(GrSc_S)^{-1}\kappa^2$, parameter used in solution for two active scalar case
a_T	$(GrSc_T)^{-1}\kappa^2$, parameter used in solution for two active scalar case
A	parameter in RDT model equation related to the turbulence time scale
A_j	eigenvector/coefficient of polynomial equation
b	$1-\kappa_3^2/\kappa^2$, parameter used in solution for two active scalar case
b'	fluctuating buoyancy
$\hat{b}$	Fourier amplitude of the buoyancy
$\hat{b}_0$	initial condition for Fourier amplitude of the buoyancy
B	Fourier amplitude of the buoyancy in RDT model equations
$\hat{B}$	nonlinear term in buoyancy equation
$\hat{B}_j$	identifier for individual components of nonlinear term in buoyancy equation where j corresponds to individual components of $\hat{B}$
B^*	coefficient in RDT model equation
B_j	eigenvector/coefficient of polynomial equation
$c_{j\varepsilon}$	specified coefficients in k-ε model where j = 1, 2, or 3
c_μ	proportionality constant for eddy viscosity in k-ε model
C	parameter in RDT model equations related to the frequency
C_j	eigenvector/coefficient of polynomial equation
D	molecular diffusivity
DIA	direct interaction approximation
DNS	direct numerical simulations
D_T	turbulent eddy diffusivity
D_j	eigenvector/coefficient of polynomial equation
E	parameter in RDT model equations

E_3	one dimensional energy spectrum
E_{33}	three dimensional energy spectrum
$E_{33}(\kappa,0)$	$\left[E(k)\left(1-\kappa_3^2/\kappa^2\right)\right]/\left[4\pi\kappa^2\right]$, initial energy spectrum
E_{b3}	cospectrum of vertical velocity and density
E_{S3}	cospectrum of vertical velocity and salinity
E_{T3}	cospectrum of vertical velocity and temperature
$E(k)$	energy spectrum function
EDQNM	eddy damped quasi-normal Markovian
F'	arbitrary fluctuating function
f_j	$\Gamma_T/\sigma_j + a_T$ parameter used in solution for two active scalar case
F	arbitrary function
F_b	dimensionless buoyancy flux
F_j	vertical flux where $j = T$ or S
Fr	$u/NL = Ri^{-1/2}$, Froude number
g	acceleration due to gravity
g_j	$\Gamma_S/\sigma_j + a_S$, parameter used in solution for two active scalar case
G	arbitrary function
Gr	$NL^2/\nu = Re/Fr$, Grashof number
H	depth of tank
i	$\sqrt{-1}$, imaginary number
I	arbitrary integrand from method of stationary phase
j	index used in summations, j = 1, 2, 3 are streamwise, spanwise and vertical directions, respectively
k	wavenumber; standard notation for turbulent kinetic energy for k-ε model (Appendix B)
k_n	wavenumber in n-direction
$\boldsymbol{k}$	wavenumber vector
KE_0	initial kinetic energy
K_ρ	eddy diffusivity of density

KH	Kevlahan and Hunt (1997)
L	length scale
L_0	length scale of largest eddy
L_3	longitudinal length scale in the vertical direction
L_f	longitudinal integral scale (YW notation)
L_u	integral length scale using velocity fluctuations in the u direction (YW notation)
ℓ	longitudinal integral length scale
LHDI	Lagrangian history direct interaction
LVA	Lienhard and Van Atta (1990)
m	Einstein index, holds similar values as j
M	grid mesh size in stratified flow experiments
M^*	coefficient in RDT model equation
$\hat{M}_j$	nonlinear term in momentum equation
$M_{n,m}$	identifier for individual components of nonlinear term $\hat{M}$ corresponding to n row, m column of matrix
n	Einstein index, holds similar values as j
n	unit vector normal to surface
N	$\left[-\left(g/\rho_0\right)d\bar{\rho}/dx_3\right]^{1/2}$, buoyancy frequency
$O(n)$	order n solution using perturbation method
p'	fluctuating pressure
$\hat{p}$	Fourier amplitude of pressure
P	parameter in RDT model equation related to the Grashof number
$\hat{P}$	$k_m\hat{u}_j * k_j\hat{u}_m / k^2$, convolution term in Poisson equation
p_1	$Gr^{-1}(1+Sc^{-1})\kappa^2$, parameter used in buoyancy flux equation
p_2	$Gr^{-1}(1-Sc^{-1})\kappa^2$, parameter used in buoyancy flux equation
Pe	uL/D, Péclet number
PE_0	initial potential energy
ΔPE	change in mean potential energy

q	$\left(4\sin^2\theta - p_2^2\right)^{1/2}$, parameter used in buoyancy flux equation
Q	parameter in RDT model equation related to the Schmidt number
$q_0^2/2$	initial turbulent kinetic energy
r	PE_0/KE_0, energy ratio
R	parameter in RDT model equations related to the decay of the nonlinear terms
R_{ij}	flux notation in numerical model
$R_{\rho w}$	$-\overline{\rho' u_3'} \Big/ \left(\overline{\rho'^2 u_3'^2}\right)^{1/2}$, vertical flux correlation coefficient
$\hat{r}_j$	Fourier amplitude used with integrating factor for nonlinear term analysis, corresponds to the Fourier amplitude of the velocity component
Re	uL/v, Reynolds number
R_f	flux Richardson number
R_ρ	density ratio
Ri	$(NL/u)^2 = Fr^{-2}$, Richardson number
RDT	rapid distortion theory
RMS	root mean square
RNG	renormalization group
S	salinity
s	bounding surface of volume
$\hat{s}$	Fourier amplitude used with integrating factor for nonlinear term analysis, corresponds to the Fourier amplitude of the buoyancy component
Sc	v/D, Schmidt number
Sc_S	700, Schmidt number for salt
Sc_T	7, Schmidt number for heated water
t	time
t'	dimensionless eddy turnover time
T	temperature
T'	fluctuating temperature
T_{turb}	λ/u_λ, time scale of turbulence (eddy turnover time)

T_{mean}	N^{-1}, time scale of mean flow (gravitational adjustment time)
TFM	test field model
TKE	turbulent kinetic energy
u	velocity
u_0	velocity scale
u_λ	velocity scale of eddy with length λ
u'_j	fluctuating velocity component in j-direction
$\hat{u}_j$	Fourier amplitude of the velocity component in j-direction
$\hat{u}_S$	$g\beta\hat{S}/(q_0 N)$, Fourier amplitude for salt
$\hat{u}_T$	$g\alpha\hat{T}/(q_0 N)$, Fourier amplitude for temperature
$\hat{u}_{j0}$	initial conditions for Fourier amplitude of the velocity component in j-direction
U_m	mean flow velocity in m-direction
V	volume
w	$\left(1-\kappa_3^2/\kappa^2\right)^{1/2} = \sin\theta$, parameter in nonlinear term analysis
W	Fourier amplitude of the velocity in RDT model equations
x_j	spatial coordinate in j-direction, where j = 1, 2, 3 and correspond to x, y and z directions, respectively
x	spatial vector that refers to coordinate system that follows mean flow
YW	Yoon and Warhaft (1990)

Greek Symbols

α	thermal expansion coefficient
α_j	parameter used in solution for two active scalar case
β	haline contraction coefficient
β_j	$f_j\alpha_j$, parameter used in solution for two active scalar case with no sum on j
γ_1, γ_2	spatial phase distributions for initial conditions in nonlinear evaluation
γ_j	$g_j\alpha_j$, parameter used in solution for two active scalar case with no sum on j
Γ	strain rate

Γ_S	$-1/(R_\rho+1)$, parameter used in solution for two active scalar case
Γ_T	$-R_\rho/(R_\rho+1)$, parameter used in solution for two active scalar case
δ_{j3}	Kronecker delta; equal to 1 when $j = 3$ and 0 when $j \neq 3$
ε	dissipation rate of turbulent kinetic energy
ζ	arbitrary transition value between local and global nonlinear sources
η	mixing efficiency
η_∞	$0.5(1-2rSc)/(1+Sc)$, mixing efficiency as $Gr \to \infty$ for one active scalar
θ	spherical coordinate angle measured from the k_3 axis (in vertical plane)
θ_S	stationary point used in method of stationary phase
κ	dimensionless wavenumber
$\boldsymbol{\kappa}$	dimensionless wavenumber vector
κ_j	dimensionless wavenumber in j-direction
λ	length scale of eddy
ν	kinematic viscosity
ν_t	turbulent eddy viscosity
ξ	phase in RDT model equation
ρ	density
ρ'	fluctuating density
ρ_0	reference density
$\bar{\rho}$	background density
σ	eigenvalues/roots of polynomial equation
σ_t	specified coefficient in k-ε model
τ	Nt, dimensionless time
ϕ	spherical coordinate angle measured from the k_1 axis (in horizontal plane)
χ	parameter used to develop initial conditions in nonlinear evaluation
ψ	parameter used to develop initial conditions in nonlinear evaluation
$\hat{\omega}_j$	Fourier amplitude of the vorticity in j-direction
Ω	velocity component distribution for initial conditions in nonlinear evaluation

Other notation

$-\overline{u'_m u'_n}$	Reynolds stress
$(g/\rho_0)\overline{\rho' u'_3}$	vertical buoyancy flux

ACKNOWLEDGMENTS

I would like to acknowledge and thank the National Science Foundation (Grant 1034221) for providing the financial support for me to complete research on this project.

Completion of this research would not have been possible without my advisor, Dr. Chris Rehmann. I am particularly grateful for his guidance and patience as I meticulously worked through papers, calculations, and codes and expressing faith in me that I am capable of pursuing doctoral work. I recall telling Dr. Rehmann over three years ago that I wanted to pursue graduate work because I wasn't feeling challenged enough in my current position; the research experience he provided me with definitely filled that void. I have learned a tremendous amount over the past two years about an incredibly difficult topic – all from the greatest teacher I know. I would also like to thank my thesis committee members, Dr. Roy Gu and Dr. Hui Hu for taking time to provide suggestions and comments.

While my family provided absolutely no help when asked about differential equations or turbulence, thankfully they were able to help out in other ways! Without the support and reassurance from my husband, Jesse, I would have never quit my job and left him in Milwaukee to move back to Iowa and get this degree. I am also thankful that I have the best parents in the world who support these crazy decisions; I would not be where I am today without them. A special thanks goes to my Aunt Corrine and Uncle Fred who opened their home to me, and occasional visits from Jesse and Stella, during my time back here at Iowa State University.

I cannot forget about those who have cycled through the 480 Town Engineering Building office – especially Greta Schmalle and Joel Sikkema, the best officemates ever. My graduate experience wouldn't have been the same without these two and the friendships we developed. And now, thanks to Jake Pichelmann for providing weekend and late night company as I worked to finish my thesis, and Cindy Maroney, my voodoo math queen. I also to want to thank all of the new friends I have made here, especially Beth Hartmann, Hannah Bygd and Laura Lara – they will be missed.

ABSTRACT

Mixing efficiency and nonlinear interactions in stratified turbulence were studied using rapid distortion theory (RDT). Mixing efficiency was predicted in strongly stratified flows for both one and two active scalars. The former used results of Hanazaki and Hunt (1996), while a new analytical solution was derived for the latter. Mixing efficiencies depend on the Schmidt number *Sc*, Grashof number *Gr*, and density ratio R_ρ. A decrease in the mixing efficiency was observed as *Sc* increased for the one scalar case and as R_ρ decreased for the two scalar case. RDT was also extended in an attempt to better predict behaviors in moderately stratified flows. Extensions using eddy viscosities, simulations, and modification of RDT input parameters were attempted and compared to experimental data, but magnitude and peak timing discrepancies in the vertical flux correlation coefficient curves remained. A different attempt at extending RDT was made by deriving expressions for the neglected nonlinear terms using an approach similar to Kevlahan and Hunt (1997). A model system including the expected form of the nonlinear terms showed that adjustment of coefficients in the nonlinear term had the ability to influence the period and decay of turbulent parameters.

CHAPTER 1: GENERAL INTRODUCTION

Significance and Problem Definition

Stratification exists naturally in many geophysical flows. For example, lakes can be thermally stratified due to seasonal air temperature changes, and oceans can be stratified by heat, salt, or both depending on geographic location. Differences in the density of lighter warm water and the heavier cold or saline water lead to the formation of layers, and therefore a density gradient. The presence of stratification within a flow reduces the ability of scalars like nutrients, heat, or oxygen to be transported between layers (Fernando, 1991; Wuest et al., 1996).

Engineers, limnologists, and oceanographers are often interested in quantifying how much transport, or mixing, occurs between layers of a stratified water body. This transport is quantified through the vertical density flux. In practice it is difficult to measure the vertical density flux directly, so often another parameter, the mixing efficiency, is estimated and used to obtain the flux. A constant mixing efficiency value of approximately 20% is generally used for lake or ocean applications (Ferrari and Polzin, 2005; Ravens et al., 2000). Simulations and laboratory experiments show that the mixing efficiency increases with stratification up to a maximum value (Rehmann and Koseff, 2004) and also decreases as the fluid becomes less diffusive (Rehmann and Koseff, 2004; Stretch et al., 2010). However, the dependency of the mixing efficiency on molecular effects, in terms of the Schmidt number Sc and Grashof number Gr, is not well understood. A better understanding of how fluid properties and flow conditions influence the mixing efficiency will lead to better estimates of the vertical flux.

Turbulence models are based on equations for the conservation of mass and conservation of momentum and are commonly used to predict vertical fluxes or parameters like the mixing efficiency. Because these equations are nonlinear by nature and the system is not closed, assumptions and approximations must be applied for solutions to be reached. One such model, rapid distortion theory (RDT), can be applied to stratified flows. However, RDT neglects nonlinear terms present in the conservation equations by assuming that eddies are rapidly distorted by gravity before interacting with each other.

Turbulent events result in an energy cascade from large scale to small scale eddy structures where nonlinear interactions naturally occur during this process. While these interactions are recognized as having the potential to influence the vertical density flux, and consequently parameters like the mixing efficiency, quantitatively accounting for nonlinear interactions in turbulence models presents a mathematical challenge. In addition, many environmental flows existing in nature are moderately stratified where nonlinear motions have a greater influence than in strongly stratified flows (Imberger and Ivey, 1991). Quantitative representation of neglected nonlinear terms could improve the ability of turbulence models like RDT to better predict mixing and transport in geophysical flows.

Objectives

This work aims to (i) understand how mixing efficiency depends on fluid characteristics and flow types and (ii) evaluate rapid distortion theory with the expected form of the nonlinear terms to understand role of nonlinear effects. Mixing efficiencies will be determined and evaluated using analytical solutions for one and two active scalars, while an approach similar to Kevlahan and Hunt (1997) will be used to develop expressions for nonlinear terms neglected from rapid distortion theory.

Thesis Organization

Each of the following chapters pertains to different, yet related, aspects of turbulence in stratified flows. Chapter 2 includes a draft of the paper regarding mixing efficiency predictions using RDT which will be submitted to *Dynamics of Atmospheres and Oceans*. The extension of RDT through the addition of the neglected nonlinear terms to better predict characteristics of moderately stratified flows is included in Chapter 3. General conclusions of work completed and recommendations for future research are presented in Chapter 4.

CHAPTER 2: ANALYTICAL MODEL OF MIXING EFFICIENCY OF TURBULENCE IN A STRONGLY FLOW

A paper submitted to *Dynamics of Atmospheres and Oceans*

Jennifer Jefferson[1,2] and Chris Rehmann[1,3]

Abstract

The mixing efficiency of unsheared homogeneous turbulence in flows stratified by one or two active scalars was calculated with rapid distortion theory (RDT). For the case with one scalar the mixing efficiency η depends on the Schmidt number $Sc = \nu/D$ and the Grashof number $Gr = NL^2/\nu$, where ν is the kinematic viscosity, D is the molecular diffusivity, N is the buoyancy frequency, and L is proportional to the longitudinal integral length scale. For the case with two scalars, the efficiency also depends on the density ratio R_ρ, which compares the density difference caused by temperature and the density difference caused by salt. In the one scalar case when Gr is large, η decreases as Sc increases. The mixing efficiency increases with Gr up to a maximum value, as shown in numerical simulations and experiments. The maximum mixing efficiency of approximately 30% for low Sc is consistent with simulations, while the maximum efficiency of 6% for heated water is consistent with laboratory measurements. However, RDT underpredicts the maximum efficiency for saltwater and also the value of Gr at which the efficiency becomes constant. The predicted behavior of the mixing efficiency for two active scalars is similar to that for one scalar, and the efficiency decreases as R_ρ decreases, as in experiments and semi-empirical models. These calculations show that results from simulations with low Sc likely overestimate the efficiency of turbulence in strongly stratified flows in lakes and oceans.

Introduction

Understanding the transport of scalars such as heat, salt, nutrients, and pollutants in environmental flows is important for predicting climate, water quality, and the health of

[1] Graduate student and Associate Professor, respectively, Department of Civil, Construction and Environmental Engineering, Iowa State University.
[2] Primary researcher and author.
[3] Author for correspondence.

aquatic life. Because fluxes are difficult to measure directly, a common approach is to use a mixing efficiency to estimate an eddy diffusivity and obtain vertical fluxes (Osborn, 1980). Often a constant value is assumed for measurements in the ocean (Ferrari and Polzin, 2005) and lakes (Ravens et al., 2000). However, mixing and its efficiency depend on factors such as the strength of stratification, molecular diffusivity of the scalar, and the process generating the turbulence (Turner 1973, chapters 9-10), and questions remain about the magnitude of the mixing efficiency and its behavior in strong stratification. Here we use rapid distortion theory (RDT) to explore the behavior of the mixing efficiency in flows with strong stratification caused by either a single scalar or two stably-stratified scalars.

Several quantities called mixing efficiency are used to study stratified flows, but their definitions vary. In devising a method to estimate the eddy diffusivity from measurements of turbulence microstructure, Osborn (1980) defined a flux Richardson number R_f as the vertical buoyancy flux $(g/\rho_0)\overline{\rho' u_3'}$ divided by the production of turbulent kinetic energy (TKE), where g is the acceleration due to gravity, ρ_0 is a reference density, ρ' is the fluctuating density, u_3' is the fluctuating velocity in the vertical (or x_3) direction, and the overbar denotes an average. Ivey and Imberger (1991) generalized this definition of mixing efficiency by comparing the buoyancy flux to all sources of TKE. Because the flux Richardson number measures the relative importance of terms in the TKE balance, it can vary widely during the evolution of a single turbulent event. For example, during restratification, which is a key feature of decaying turbulence in a stratified flow (Lienhard and Van Atta, 1990), it is negative.

Another definition of mixing efficiency depends on the change in mean potential energy ΔPE during a turbulent event. This change is a key quantity of interest to oceanographers (Gregg, 1987) because it measures the net effect of downgradient and upgradient fluxes on the background density profile. In experiments with a grid towed through a linearly stratified fluid, mixing efficiency has been defined as the ratio of ΔPE, which is computed from density profiles measured before the tow and after the turbulence decays, to the work done to create the turbulence (Rehmann and Koseff, 2004). A similar definition can be applied to numerical simulations of homogeneous turbulence even though

the background density gradient does not change: Stretch et al. (2010) neglected fluxes from molecular diffusion along the background gradient and computed ΔPE by integrating the buoyancy flux over the life of the turbulence, and they computed a mixing efficiency η as ΔPE divided by the initial TKE $q_0^2/2$:

$$\eta = \frac{\int_0^\infty \frac{g}{\rho_0}\overline{\rho' u_3'}\,\mathrm{d}t}{q_0^2/2}, \tag{2.1}$$

where t is time. We use both this definition and the symbol η to distinguish it from the flux Richardson number based on terms in the TKE equation.

The mixing efficiency depends on the strength of the stratification and the molecular diffusivity of the stratifying agent. In experiments with towed grids, the former is quantified by a Richardson number Ri formed with length and velocity scales of the grid and the buoyancy frequency $N = \left[-(g/\rho_0)d\bar{\rho}/dx_3\right]^{1/2}$, while the latter is quantified by a Prandtl number or Schmidt number $Sc = \nu/D$, where ν is the kinematic viscosity and D is the molecular diffusivity. Mixing efficiencies are small at low Ri and rise to a peak of about 6% for grid turbulence in salt-stratified fluids and temperature-stratified fluids, which have Sc_S = 700 and Sc_T = 7, respectively (Barrett and Van Atta, 1991; Britter, 1985; Rehmann and Koseff, 2004; Rottman and Britter, 1986). Simulations by Stretch et al. (2010) for Sc = 0.5 follow a similar trend for low Ri but reach a peak efficiency of about 5 times larger than observed in the experiments. Stretch et al. (2010) proposed that accounting for the energy used to generate surface and internal waves in the experiments would increase the efficiency and reduce the difference. Also, η decreased with increasing Sc in their full simulations with Sc = 0.5, 1, and 2 and simulations with higher Sc that did not include nonlinear terms, but because the decrease occurs at high Ri, they argued that wave generation causes the peak efficiency differences.

When the flow has stable distributions of two or more active scalars, the mixing efficiency can depend on another parameter. Field experiments (Nash and Moum, 2002), laboratory experiments (Jackson and Rehmann, 2003b; Martin and Rehmann, 2006), numerical simulations (Gargett et al., 2003; Smyth et al., 2005), and theoretical models

(Jackson and Rehmann, 2009) have shown that in strongly stratified flows a scalar with larger diffusivity, such as temperature, can be transported at larger rates than a scalar with smaller diffusivity, such as salt. This differential diffusion, which is different from double diffusion, causes the mixing efficiency to depend on the fraction of the density gradient caused by each scalar which is measured by the density ratio R_ρ:

$$R_\rho = -\frac{\alpha dT / dx_3}{\beta dS / dx_3} \tag{2.2}$$

where T is temperature, S is salinity, α is the thermal expansion coefficient, β is the haline contraction coefficient. When the transport of temperature exceeds the transport of salt, the mixing efficiency will increase as more of the stratification is caused by temperature—that is, when R_ρ increases (Jackson and Rehmann, 2003a). Laboratory experiments support this intuition: At low Ri, mixing efficiencies are similar for both low and high R_ρ in more weakly stratified flows, but for higher Ri, the mixing efficiencies differ. In particular, in the experiments of Jackson and Rehmann (2003b) and Martin and Rehmann (2006), the maximum efficiency was approximately 4% for R_ρ = 0.4–0.8 but only 2.5% for R_ρ = 0.02–0.04.

We use an analytical model for unsheared homogeneous turbulence in a strongly stratified fluid to examine the magnitude and behavior of the mixing efficiency. The approach, rapid distortion theory, reproduces key features of turbulence in strongly stratified flows with one scalar (Hanazaki and Hunt, 1996) and two scalars (Jackson et al., 2005), and it allows parameters to be varied more easily than in direct numerical simulations. We compute the mixing efficiency with RDT for one and two scalar flows in the next section, then present the results and discuss the assumptions, relation to previous work, and applications before summarizing the main findings.

Theory[4]

Rapid distortion theory uses linearized equations for fluctuating velocities and scalars. This approximation results from assuming that eddies are distorted by gravitational adjustment before they can interact with each other. Hanazaki and Hunt (1996) quantified

[4] Matlab codes developed and used for one and two scalar cases are found in Appendix A.

this assumption by requiring that the Froude number $Fr_\lambda = u_\lambda/N\lambda << 1$, where λ and u_λ are length and velocity scales of an eddy. A low value of $Fr = q_0 / N\ell$, where ℓ is the longitudinal integral length scale, ensures small eddy Froude numbers when the Reynolds number *Re* is low or moderate, but when the *Re* is large, the Froude number criterion can be violated at high wavenumbers (Hanazaki and Hunt, 1996). Rapid distortion theory can also become less accurate at large times when the vortex mode, nonlinear motions with large time scales (Riley and Lelong, 2000), appears (Hanazaki and Hunt, 2004). As Jackson and Rehmann (2009) discussed, the vortex mode appears in experiments at dimensionless time $\tau = Nt = 20–30$.

Computing the mixing efficiency with equation (2.1) requires solving the equations for the vertical component of momentum and the scalars. For homogeneous turbulence with no mean velocity, the equations for the Fourier amplitudes of the vertical velocity, temperature, and salinity can be adapted from those in Jackson and Rehmann (2009):

$$\frac{d\hat{u}_3}{d\tau} = \left(\frac{\kappa_3^2}{\kappa^2} - 1\right)\left(\hat{u}_S - \hat{u}_T\right) - Gr^{-1}\kappa^2\hat{u}_3, \tag{2.3}$$

$$\frac{d\hat{u}_T}{d\tau} = -\frac{R_\rho}{R_\rho + 1}\hat{u}_3 - \left(GrSc_T\right)^{-1}\kappa^2\hat{u}_T, \tag{2.4}$$

$$\frac{d\hat{u}_S}{d\tau} = \frac{1}{R_\rho + 1}\hat{u}_3 - \left(GrSc_S\right)^{-1}\kappa^2\hat{u}_S \tag{2.5}$$

where $\hat{u}_T = g\alpha\hat{T}/(q_0 N)$, $\hat{u}_S = g\beta\hat{S}/(q_0 N)$, and $\hat{u}_3$ is the dimensional Fourier amplitude of the vertical velocity normalized by q_0. The vertical wavenumber κ_3 and the magnitude κ of the wavenumber vector are made dimensionless by the length scale *L*, which is related to the longitudinal integral length scale through the relationship $L = (\pi/2)^{-1/2}\ell$. Aside from the density ratio and the Schmidt numbers for temperature and salinity, another key dimensionless parameter is the Grashof number $Gr = NL^2/\nu$. Jackson et al. (2005) related *Gr* to ε, the rate of dissipation of TKE, normalized by νN^2; the parameter $\varepsilon/\nu N^2$ is frequently used as a measure of the intensity of turbulence in stratified water bodies. Once the Fourier coefficients are obtained from (2.3)–(2.5), cospectra of vertical velocity and scalars can be computed with

$$E_{T3}(\boldsymbol{\kappa},t)=\tfrac{1}{2}\left(\overline{\hat{u}_3\hat{u}_T^*}+\overline{\hat{u}_3^*\hat{u}_T}\right)\qquad\text{and}\qquad E_{S3}(\boldsymbol{\kappa},t)=\tfrac{1}{2}\left(\overline{\hat{u}_3\hat{u}_S^*}+\overline{\hat{u}_3^*\hat{u}_S}\right)\tag{2.6}$$

where the star indicates a complex conjugate. Integrating over all wavenumbers yields the vertical fluxes of temperature and salt

$$F_T=-\overline{u_3'u_T'}=\int E_{T3}\mathrm{d}^3\boldsymbol{\kappa}\qquad\text{and}\qquad F_S=\overline{u_3'u_S'}=\int E_{S3}\mathrm{d}^3\boldsymbol{\kappa}\,,\tag{2.7}$$

so that the buoyancy flux can be expressed as $(g/\rho_0)\overline{\rho'u_3'}=q_0^2NF_b=q_0^2N(F_T+F_S)$, where F_b is the dimensionless buoyancy flux.

The mixing efficiency was computed for flows stratified by one scalar and two scalars. The one scalar case can be obtained by setting $R_\rho = 0$ and $\hat{u}_T=0$ in (2.3)–(2.5). For this case, the work of Hanazaki and Hunt (1996), who solved for initially isotropic turbulence, can be used to write the dimensionless buoyancy flux as

$$F_b=\tfrac{1}{2}\int_0^\infty\!\!\int_0^\pi E(\kappa)e^{-p_1\tau}\frac{\sin^3\theta}{q^2}\Big[(1-2r)q\sin q\tau-(1+2r)\,p_2\left(1-\cos q\tau\right)\Big]\mathrm{d}\theta\mathrm{d}\kappa\tag{2.8}$$

where $p_1 = Gr^{-1}(1+Sc^{-1})\kappa^2$, $p_2 = Gr^{-1}(1-Sc^{-1})\kappa^2$, $q=\left(4\sin^2\theta-p_2^2\right)^{1/2}$, $r = PE_0/KE_0$ is the initial potential energy divided by the initial kinetic energy, respectively, and θ is the angle between the wavenumber vector and the vertical direction. The dimensionless energy spectrum function is taken to be

$$E(\kappa)=\frac{1}{3\sqrt{2\pi}}\kappa^4e^{-\kappa^2/2}.\tag{2.9}$$

Then from (2.1), the mixing efficiency for the one scalar case is

$$\eta=\eta_\infty\int_0^\infty\!\!\int_0^\pi\frac{E(\kappa)\sin^3\theta}{\sin^2\theta+\kappa^4/(Gr^2Sc)}\mathrm{d}\theta\mathrm{d}\kappa\tag{2.10}$$

where

$$\eta_\infty=\frac{1}{2}\left(\frac{1-2rSc}{1+Sc}\right).\tag{2.11}$$

Either one of the two integrals in (2.10) can be evaluated in closed form, but integrating both numerically is simpler to obtain values of the efficiency.

The mixing efficiency for flows with stable distributions of two scalars is computed in a similar way. The Fourier coefficients are computed from equations (2.3)–(2.5) by assuming solutions of the form

$$\hat{u}_3 = \sum_{j=1}^{3} A_j \exp\left(\sigma_j \tau\right), \quad \hat{u}_T = \sum_{j=1}^{3} B_j \exp\left(\sigma_j \tau\right), \quad \text{and} \quad \hat{u}_S = \sum_{j=1}^{3} C_j \exp\left(\sigma_j \tau\right), \tag{2.12}$$

where A_j, B_j, and C_j are coefficients and σ_j are the roots of

$$\sigma^3 + (a + a_S + a_T)\sigma^2 + (aa_S + aa_T + a_S a_T + b)\sigma + aa_S a_T + b(a_T \Gamma_S - a_S \Gamma_T) = 0. \tag{2.13}$$

Additional variables in (2.13) are defined as $a = Gr^{-1}\kappa^2$, $a_T = (GrSc_T)^{-1}\kappa^2$, $a_S = (GrSc_S)^{-1}\kappa^2$, $b = 1 - \kappa_3^2 / \kappa^2$, $\Gamma_T = -R_\rho/(R_\rho+1)$, and $\Gamma_S = -1/(R_\rho+1)$. Explicit expressions for the three roots—which consist of either three real roots or one real root and a complex conjugate pair—are cumbersome, but can be obtained with the procedure in section 1.11 of the National Institute of Standards and Technology (NIST) Digital Library of Mathematical Functions (2012). The coefficients can be related by substituting (2.12) into (2.4) and (2.5):

$$B_j = \frac{\Gamma_T A_j}{\sigma_j + a_T} = f_j A_j \qquad \text{and} \qquad C_j = \frac{\Gamma_S A_j}{\sigma_j + a_S} = g_j A_j \tag{2.14}$$

which hold for j = 1, 2, and 3. Applying the initial conditions gives

$$\hat{u}_3(\boldsymbol{\kappa}, 0) = \hat{u}_{30} = A_1 + A_2 + A_3 \tag{2.15}$$

$$\hat{u}_T(\boldsymbol{\kappa}, 0) = \hat{u}_{T0} = f_1 A_1 + f_2 A_2 + f_3 A_3, \tag{2.16}$$

$$\hat{u}_S(\boldsymbol{\kappa}, 0) = \hat{u}_{S0} = g_1 A_1 + g_2 A_2 + g_3 A_3. \tag{2.17}$$

The solution of the system (2.15)–(2.17) is

$$A_1 = \hat{u}_{30} - A_2 - A_3, \tag{2.18}$$

$$A_2 = \frac{1}{f_2 - f_1}\left[\hat{u}_{T0} - f_1 \hat{u}_{30} - A_3(f_3 - f_1)\right], \tag{2.19}$$

$$A_3 = \frac{(f_1 g_2 - f_2 g_1)\hat{u}_{30} + (g_1 - g_2)\hat{u}_{T0} - (f_1 - f_2)\hat{u}_{S0}}{f_1 g_2 - f_1 g_3 - f_2 g_1 + f_2 g_3 + f_3 g_1 - f_3 g_2}. \tag{2.20}$$

After the Fourier coefficients are assembled with (2.12) and (2.18)–(2.20), the spectra can be computed with (2.6); for simplicity the initial temperature and salinity fluctuations are assumed to be zero:

$$
\begin{aligned}
E_{T3}(\boldsymbol{\kappa},t) = \tfrac{1}{2}E_{33}(\boldsymbol{\kappa},0)\Big[&\left(\alpha_1\beta_1^* + \alpha_1^*\beta_1\right)e^{(\sigma_1+\sigma_1^*)t'} + \left(\alpha_1\beta_2^* + \alpha_2^*\beta_1\right)e^{(\sigma_1+\sigma_2^*)t'} \\
&\left(\alpha_1\beta_3^* + \alpha_3^*\beta_1\right)e^{(\sigma_1+\sigma_3^*)t'} + \left(\alpha_2\beta_2^* + \alpha_2^*\beta_2\right)e^{(\sigma_2+\sigma_2^*)t'} \\
&\left(\alpha_2\beta_1^* + \alpha_1^*\beta_2\right)e^{(\sigma_2+\sigma_1^*)t'} + \left(\alpha_3\beta_1^* + \alpha_1^*\beta_3\right)e^{(\sigma_3+\sigma_1^*)t'} \\
&\left(\alpha_3\beta_3^* + \alpha_3^*\beta_3\right)e^{(\sigma_3+\sigma_3^*)t'} + \left(\alpha_2\beta_3^* + \alpha_3^*\beta_2\right)e^{(\sigma_2+\sigma_3^*)t'} \\
&\left(\alpha_3\beta_2^* + \alpha_2^*\beta_3\right)e^{(\sigma_3+\sigma_2^*)t'}\Big],
\end{aligned}
\tag{2.21}
$$

$$
\begin{aligned}
E_{S3}(\boldsymbol{\kappa},t) = \tfrac{1}{2}E_{33}(\boldsymbol{\kappa},0)\Big[&\left(\alpha_1\gamma_1^* + \alpha_1^*\gamma_1\right)e^{(\sigma_1+\sigma_1^*)t'} + \left(\alpha_1\gamma_2^* + \alpha_2^*\gamma_1\right)e^{(\sigma_1+\sigma_2^*)t'} \\
&\left(\alpha_1\gamma_3^* + \alpha_3^*\gamma_1\right)e^{(\sigma_1+\sigma_3^*)t'} + \left(\alpha_2\gamma_2^* + \alpha_2^*\gamma_2\right)e^{(\sigma_2+\sigma_2^*)t'} \\
&\left(\alpha_2\gamma_1^* + \alpha_1^*\gamma_2\right)e^{(\sigma_2+\sigma_1^*)t'} + \left(\alpha_3\gamma_1^* + \alpha_1^*\gamma_3\right)e^{(\sigma_3+\sigma_1^*)t'} \\
&\left(\alpha_3\gamma_3^* + \alpha_3^*\gamma_3\right)e^{(\sigma_3+\sigma_3^*)t'} + \left(\alpha_2\gamma_3^* + \alpha_3^*\gamma_2\right)e^{(\sigma_2+\sigma_3^*)t'} \\
&\left(\alpha_3\gamma_2^* + \alpha_2^*\gamma_3\right)e^{(\sigma_3+\sigma_2^*)t'}\Big].
\end{aligned}
\tag{2.22}
$$

Because the turbulence is taken to be isotropic initially, the energy spectrum is

$$
E_{33}(\kappa,0) = \frac{E(\kappa)}{4\pi\kappa^2}\left(1-\frac{\kappa_3^2}{\kappa^2}\right). \tag{2.23}
$$

The coefficients in (2.21) and (2.22) are

$$
\begin{aligned}
\alpha_1 &= 1-\alpha_2-\alpha_3, \\
\alpha_2 &= \frac{-f_1-(f_3-f_1)\alpha_3}{f_2-f_1}, \\
\alpha_3 &= \frac{f_1g_2-f_2g_1}{f_1g_2-f_1g_3-f_2g_1+f_2g_3+f_3g_1-f_3g_2},
\end{aligned}
\tag{2.24}
$$

and $\beta_j = f_j\alpha_j$ and $\gamma_j = g_j\alpha_j$ with j = 1, 2, and 3 (no sum on j). After the fluxes are computed with (2.7), the mixing efficiency can be computed with (2.1).

Results

One Active Scalar

Fluxes computed with RDT oscillate with decaying amplitude (Figure 2.1). The flux alternates between downgradient and upgradient with a period of about $3N^{-1}$, and the periods for Gr = 10 and Gr = 1,000 are similar. The amplitude of the oscillation depends strongly on Gr, which indicates the importance of viscosity: For Gr = 10, the vertical flux is small by τ =

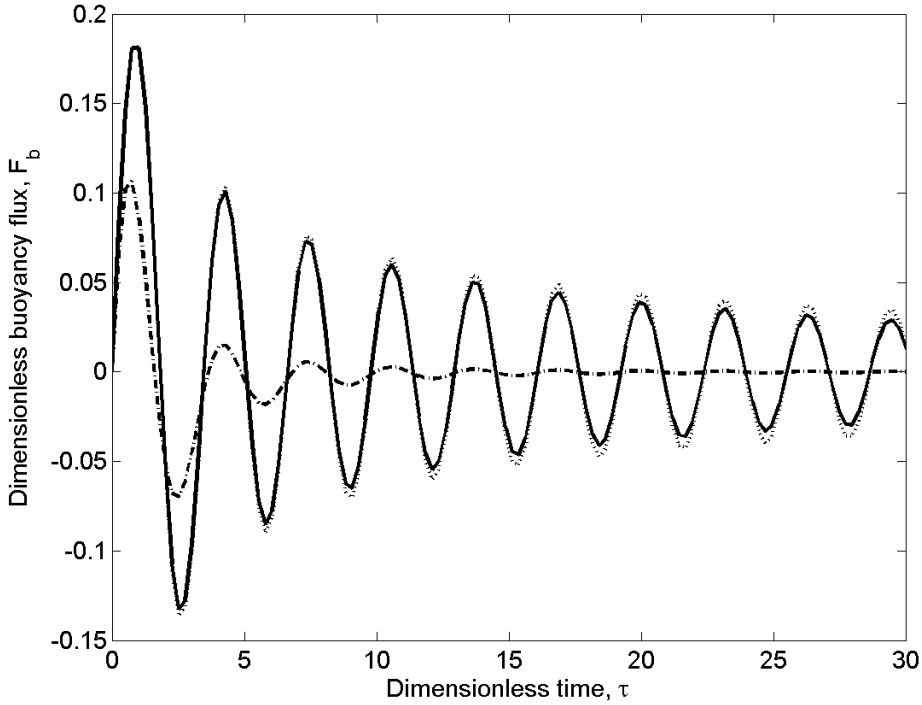

Figure 2.1: Time evolution of the buoyancy flux: —, *Sc* = 0.7 and *Gr* = 1,000; --, *Sc* = 700 and *Gr* = 1,000; – - –, *Sc* = 700 and *Gr* = 10.[5]

20, but for *Gr* = 1,000 the amplitude at $\tau = 30$ is about 6 times smaller than the maximum value during the evolution. The amplitude increases as *Sc* increases, or as effects of molecular diffusion of the stratifying agent decrease, but for higher values of Grashof number, differences caused by changes in the Schmidt number are small.

When the Grashof number is large, the mixing efficiency decreases as the Schmidt number increases (Figure 2.2). As $Gr \rightarrow \infty$, the quantity Gr^2Sc also becomes large, and the second term in the denominator in (2.10) becomes small. Then, because the integral of the energy spectrum function over all wavenumbers is ½, the mixing efficiency approaches η_∞. For no initial density fluctuations ($r = 0$), η_∞ is 0.5 for small Schmidt number, and it equals 0.25 for *Sc* = 1, which is typical of scalars used in direct numerical simulations. As *Sc* increases to values more representative of the ocean and lakes, η_∞ is smaller: for heat in water, it is about 6%, and for salt in water it is about 0.1%. As the Grashof number and

[5] Matlab code used to generate figure: VortexModeCompare.m

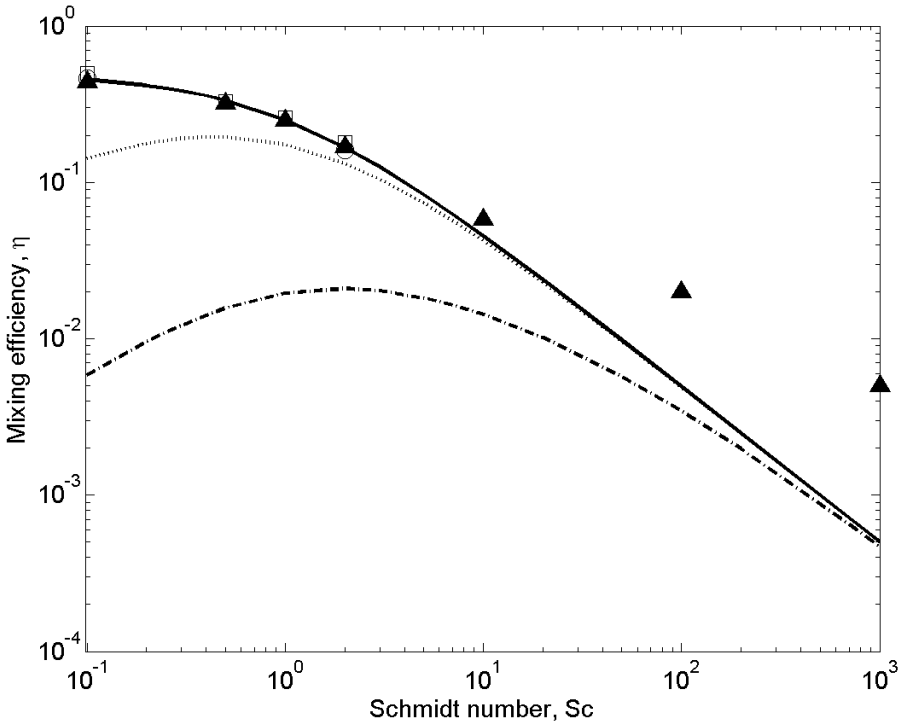

Figure 2.2: Dependence of mixing efficiency on Schmidt number for one active scalar. RDT: —, Gr = 10,000; --, Gr = 10; – - –, Gr = 1. Results from Stretch et al. (2010) for Ri = 1,000: ▲, RDT simulation—Re = 100; ○, DNS—Re = 100; □, DNS—Re = 200.[6]

Schmidt number decrease, the mixing efficiency decreases below η_∞, but as long as $Gr^2Sc > 10^4$, the mixing efficiency is within 1% of the asymptotic value η_∞.

The mixing efficiency computed with RDT matches the predictions from numerical simulations at low Schmidt number, but the quantitative agreement weakens as Sc becomes large (Figure 2.2). To compare with results from direct numerical simulations (DNS) and RDT simulations (i.e., simulations of the governing equations with nonlinear terms neglected) of Stretch et al. (2010), the Grashof number was computed as $Gr = ReRi^{1/2}$. For $Sc < 2$ efficiencies from the simulations, which have values of Gr of 3,162 and 6,324, are predicted well with the asymptotic value of the mixing efficiency for large Gr. Predictions from rapid distortion theory fall below the values from RDT simulations at higher Schmidt number; at Sc = 1,000, the value from RDT is 10 times smaller. The dependence on the

[6] Matlab code used to generate figure: Rfdriver_Fig34.m

Schmidt number is also different: Simulations show that $\eta \sim Sc^{-1/2}$ at high Sc (Stretch et al., 2010), while RDT predicts $\eta \sim Sc^{-1}$, as can be seen in (2.11) when $Sc >> 1$.

The dependence of mixing efficiency on Gr predicted using RDT is qualitatively consistent with the behavior of results from DNS, though some differences between the predictions from theory and results from previous work are apparent (Figure 2.3). As noted above, the mixing efficiency becomes a function of only Sc when Gr is large. For small Gr, the first term in the denominator of (2.10) is small, and the efficiency is approximately given by

$$\frac{\eta}{\eta_\infty} = \int_0^\infty \int_0^\pi \frac{E(\kappa)\sin^3\theta}{\kappa^4 / Gr^2 Sc} \mathrm{d}\theta \mathrm{d}\kappa = Gr^2 Sc \int_0^\infty \frac{E(\kappa)}{\kappa^4} \mathrm{d}\kappa \int_0^\pi \sin^3\theta \mathrm{d}\theta \,. \tag{2.25}$$

Results from DNS also follow a Gr^2 dependence at low Grashof number. While the maximum values of mixing efficiency from RDT are consistent with those from DNS for low Sc, RDT predicts that the mixing efficiency becomes constant at a value of Gr about 10 times smaller than that in DNS (Figure 2.3). For heated water (Sc = 7), RDT predicts the maximum mixing efficiency of about 6%, as observed in experiments, but for saltwater (Sc = 700), it produces mixing efficiencies about 10 times smaller than those from experiments. Although RDT predicts that the maximum efficiency for saltwater should be about 90 times smaller than that for heated water, the measured values lie between the limits. The measured mixing efficiencies from separate datasets increase with Gr, but efficiencies from RDT start increasing at much lower values of Grashof number.

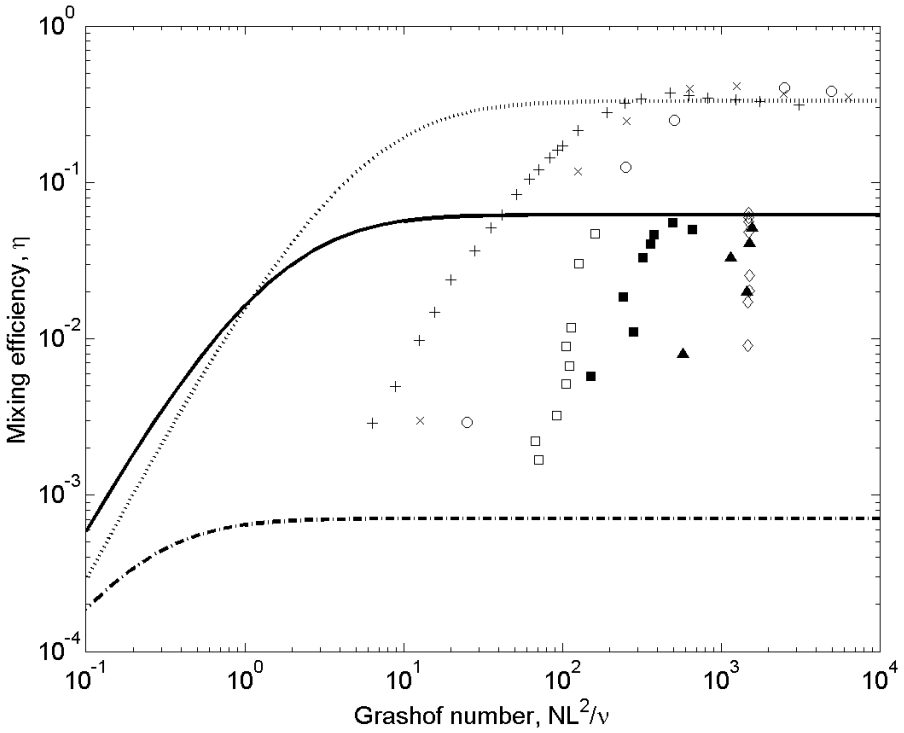

Figure 2.3: Dependence of mixing efficiency on Grashof number for one active scalar. RDT: --, Sc = 0.5; —, Sc = 7 (temperature); – - –, Sc = 700 (salt). DNS from Stretch et al. (2010) with Sc = 0.5: +, Re = 100; ×, Re = 200; ○, Re = 400. Experiments: ■, Rehmann and Koseff (2004)—salt; □, Rehmann and Koseff (2004)—temperature; ▲, Rottman and Britter (1986)—salt; ♢, Britter (1985)—salt. The length scale L in the towed-grid experiments was computed as $L = (\pi/2)^{-1/2}\ell = \xi(\pi/2)^{-1/2}M$, where M is the grid mesh and $\xi \approx 0.5$ is ℓ/M estimated at x/M = 10 in the experiments of Yoon and Warhaft (1990). [7]

Two Active Scalars

The behavior of the mixing efficiency in a flow stratified by two active scalars is similar to that in a flow with one active scalar (Figure 2.4). The efficiency increases with Gr to a constant value, and for $Gr > 1$ efficiencies for finite values of the density ratio lie between the efficiencies in the cases with each scalar alone (e.g., only temperature and only salt). The latter observation reflects the intuition and results in Jackson and Rehmann (2003a; 2003b): When transport of heat exceeds transport of salt, the mixing efficiency will be higher when more of the density gradient is due to temperature (i.e., when R_ρ is larger). One interesting quantitative result is that when salt and temperature contribute equally to the

[7] Matlab code used to generate figure: Rfdriver_Fig1.m

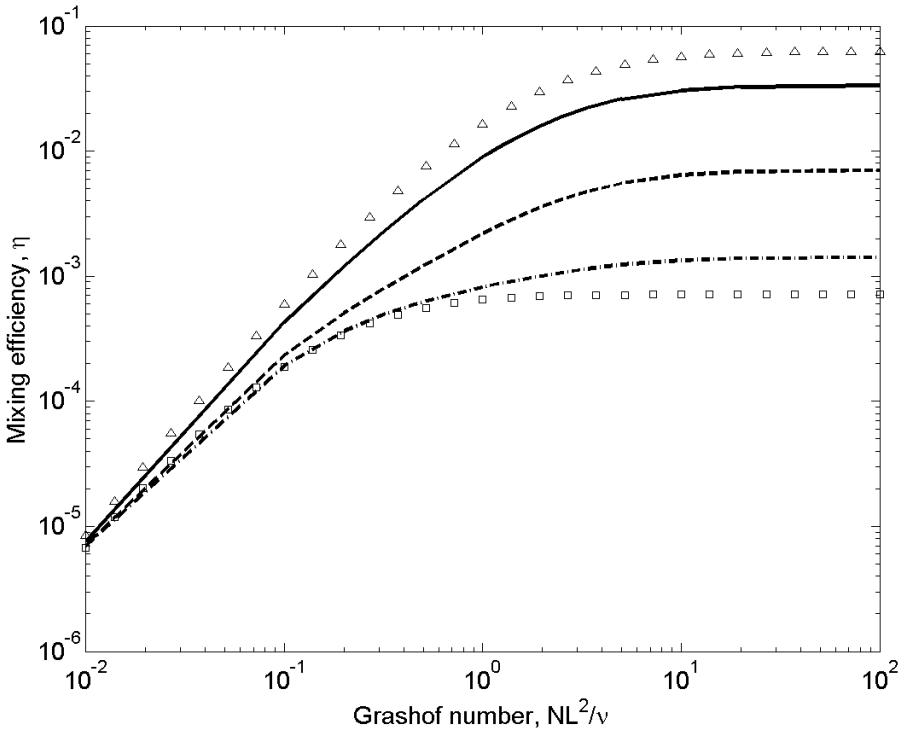

Figure 2.4: Dependence of mixing efficiency on Grashof number for two active scalars: △, $R_\rho \to \infty$ (temperature only); —, $R_\rho = 1$; --, $R_\rho = 0.1$; – - –, $R_\rho = 0.01$; □, $R_\rho = 0$ (salt only).[8]

density gradient (i.e., $R_\rho = 1$), the efficiency is much closer to the value for temperature only than the value for salt only.

The mixing efficiency computed with RDT increases with density ratio as in experiments, but quantitative agreement does not occur until R_ρ becomes large (Figure 2.5). The RDT curve shows how the efficiency varies from a flow with only salt ($\eta_\infty = 7\times10^{-4}$) to a flow with only temperature ($\eta_\infty = 0.06$); it has the same shape as the empirical expression developed by Martin and Rehmann (2006). While RDT and the empirical expression are within a factor of about 1.2 at high R_ρ, they differ by a factor of about 25 at low R_ρ. This result is consistent with the results from the one scalar case, in which RDT predict efficiencies better for heated water ($R_\rho \to \infty$) than for saltwater ($R_\rho = 0$).

[8] Matlab code used to generate figure: DDfluxdriver_Fig5.m

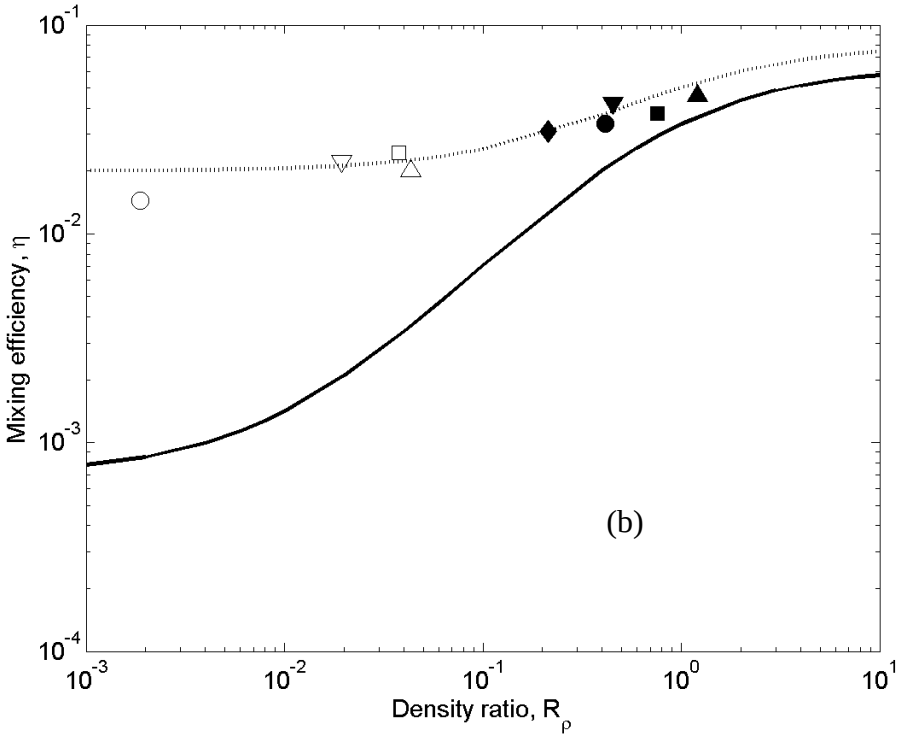

Figure 2.5: Dependence of mixing efficiency on density ratio: —, RDT for differential diffusion; --, empirical efficiency expression by Jackson and Rehmann (2003a), and experiments by Martin and Rehmann (2006): ○, $R_\rho = 0$; ▽, $R_\rho = 0.02$; □, $R_\rho = 0.04$; △, $R_\rho = 0.04$; ♦, $R_\rho = 0.21$; ●, $R_\rho = 0.41$; ▼, $R_\rho = 0.45$; ■, $R_\rho = 0.76$; ▲, $R_\rho = 1.2$. [9]

Discussion

Validity of Assumptions

The flux caused by molecular diffusion along the background density gradient was neglected in calculating the potential energy change, but in flows with less energetic turbulence it could be important. The work of Stretch et al. (2010) can be extended to show that the mean potential energy of a volume V with bounding surface s evolves according to

$$\frac{dPE}{dt} = -g\int_s x_3 \overline{\rho' u_j'} n_j ds + g\int_s x_3 D \frac{\partial \rho}{\partial x_j} n_j ds + g\int_V \overline{\rho' u_3'} dV - g\int_V D\frac{\partial \rho}{\partial x_3} dV \ , \qquad (2.26)$$

where ρ is the density and **n** is a unit vector normal to the surface. For a rectangular tank with no-flux boundaries the first two terms on the right vanish. Then, the ratio of the last two terms is

[9] Matlab code used to generate figure: DDfluxdriver_Fig6.m

$$\frac{g\int_V D\frac{\partial\rho}{\partial x_3}dV}{g\int_V \overline{\rho' u_3'}dV} \sim \frac{D\Delta\rho}{\overline{\rho' u_3'}H} = \frac{D}{\overline{\rho' u_3'}H}\frac{\rho_0 N^2 H}{g} = \frac{D}{K_\rho} \tag{2.27}$$

where H is the water depth of the tank and K_ρ is the eddy diffusivity of density. When $D/K_\rho << 1$, the background flux from molecular diffusion can be neglected. For flows with one active scalar, values of this ratio computed from the measurements of Rehmann and Koseff (2004) are less than 0.03 for temperature and 0.01 for salinity. For flows with two active scalars, the maximum values of the ratio of molecular and eddy diffusivities is 0.02 for salinity, 0.25 for temperature, and about 1 using the eddy diffusivity for density and molecular diffusivity for temperature. In the cases with $D/K_\rho \approx 1$, the background flux from molecular diffusion can increase the mixing efficiency.

Our calculation of mixing efficiency requires integrating the fluxes over all times. However, at large times the vortex mode, which RDT does not capture, can appear (Hanazaki and Hunt, 2004). If the vertical flux has decayed by $\tau \approx 30$ (Jackson and Rehmann, 2009), then the vortex mode should not affect the results significantly. The fluxes shown in Figure 2.1 suggest that if the vortex mode is important, it will occur in cases with larger *Gr*. For those cases, the predictions of RDT could be expected to be less accurate. However, the vortex mode requires the vertical velocity to be much smaller than the horizontal velocity (Hanazaki and Hunt, 2004), and for an inviscid, nondiffusive fluid RDT predicts $\left(\overline{u_3'^2}/\overline{u_1'^2}\right)^{1/2}$ < 0.5 for only about 15% of a buoyancy period early in the evolution. Therefore, the vortex mode may not a source of large uncertainty in these calculations even at high *Gr*.

Comparison with Experiments and Simulations

Mixing efficiencies for high Grashof numbers match the results from simulations of Stretch et al (2010) at low *Sc* but not at high *Sc*. Possible reasons for the differences include the presence of the vortex mode, the time of integration of the fluxes, and resolution at high *Sc*, but the discrepancy is puzzling. The vortex mode should not cause the differences because neither RDT nor the RDT simulations of Stretch et al. (2010), in which the nonlinear terms in the governing equations were neglected, can capture the vortex mode. The times over which the fluxes were integrated in computing the numerator in (2.1) differed between

our calculations and those of Stretch et al. (2010); while the theory allows fluxes to be integrated over the entire turbulent event, Stretch et al. (2010) used a finite integration time. However, at the high values of *Gr* which correspond to the simulations, RDT suggests that the fluxes are similar over a wide range of *Sc* (Figure 2.1). Therefore, if the integration time caused the differences at high *Sc*, it should also cause differences at low *Sc*. The increasing differences between results from RDT and simulations as *Sc* increases suggests that inadequate resolution in the simulations might have caused spurious diffusion. However, because the neglect of nonlinear terms prevents a cascade from occurring and smaller scales from being generated, the simulations should remain well resolved if they are well resolved initially.

Much of the difference between the predictions of RDT and results from experiments (Figure 2.3) is likely due to neglecting the nonlinear terms. Reynolds numbers based on the grid speed and mesh size were between 1,300 and 42,000 for all of the towed-grid experiments (Rehmann and Koseff, 2004); using the experiments of Yoon and Warhaft (1990) to estimate the relationships between the grid speed and TKE and between the mesh size and longitudinal integral length scale leads to Reynolds numbers $q_0\ell/\nu$ on the order of 65 to 2,100. The importance of inertia—or the effects of the nonlinear terms—is indicated by the collapse with Richardson number, which compares effects of buoyancy and inertia, evident in Figure 3 of Stretch et al. (2010) and the lack of collapse with Grashof number, which compares effects of buoyancy and viscosity, in Figure 2.3. Accounting for the effects of the neglected nonlinear terms, perhaps with the approach of Kevlahan and Hunt (1997), might improve the agreement between the theory and experiments.

The efficiency predicted by RDT remained constant over a larger range of *Gr* than either measurements from laboratory experiments or results from numerical simulations (Figure 2.3). The Grashof number for the experiments is uncertain because of the relationship between the mesh size and the longitudinal integral length scale, though the estimates of *Gr* used to plot the data in Figure 2.3 are not likely to be off by two orders of magnitude. The Grashof number for the simulations of Stretch et al. (2010) corresponds exactly to the Grashof number in the theory because they used the same initial energy spectrum function.

Therefore, the quantitative discrepancy in the dependence on *Gr* may be caused by a physical process related to the neglect of the nonlinear interactions.

Application to Limnology and Oceanography

The RDT calculations support the suggestion from Stretch et al. (2010) that Schmidt number effects can cause differences between efficiencies from DNS and efficiencies from experiments which use values of *Sc* more appropriate for lakes and oceans. The maximum mixing efficiency for $Sc = 0.5$ using DNS was about 5 times larger than the maximum mixing efficiency in experiments with $Sc = 700$ (Stretch et al., 2010). The DNS and RDT simulations showed that the efficiency decreases with *Sc*, but our RDT calculations show that the decrease is even larger than suggested by Stretch et al. (2010). Applying results from simulations with low *Sc* to strongly stratified flows in lakes and oceans would likely overestimate the mean potential energy change. Furthermore, in flows with diffusively stable distributions of salt and temperature, the density ratio must also be considered.

The asymptotic mixing efficiency η_∞ provides a good estimate of the mixing efficiency for strongly stratified flows in lakes and oceans. As shown in the Results section, the efficiency is within about 1% of η_∞ when $Gr^2Sc > 10^4$. For temperature-stratified flows, that condition corresponds to $Gr > 40$ or $L > 6(\nu/N)^{1/2}$, while for salt-stratified flows, it corresponds to $Gr > 4$ or $L > 2(\nu/N)^{1/2}$. Many oceanic flows—such as flow in the thermocline, abyssal ocean, and bottom boundary layer on the continental shelf—have $N > 10^{-3}$ rad/s (Moum, 1997). Therefore, as long as $L > 20$ cm, the simple expression given by η_∞ can be used to estimate the efficiency. Many flows observed in lakes and oceans have Grashof numbers large enough that the efficiency is approximately η_∞ (Figure 2.6). While most of the flows in Figure 2.6 have temperature stratification with $Gr > 40$ or salt stratification with $Gr > 4$, the mixing efficiency of turbulence in the hypolimnion and thermoclines of lakes and ocean would depend on the Grashof number. Some caution should be used, however, because the comparison with DNS and laboratory experiments suggests that RDT underestimates the value of *Gr* at which the efficiency becomes constant.

Many of the flows in Figure 2.6 have moderate stratification, or turbulent Froude numbers close to one. However, rapid distortion theory requires strong stratification, or $Fr << 1$. Although some of the laboratory experiments and DNS have low Froude number, the

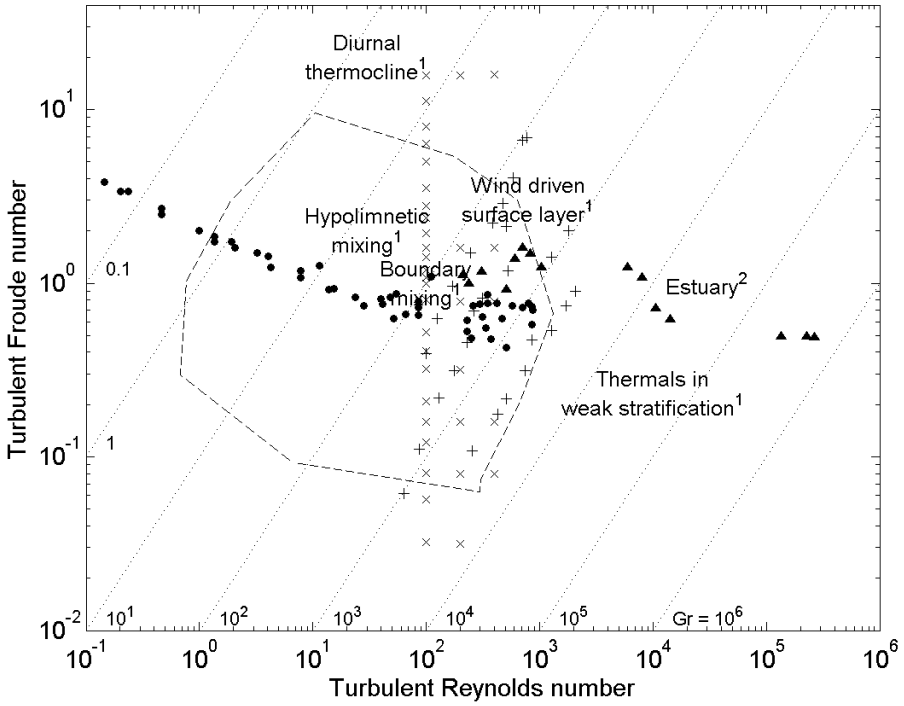

Figure 2.6: Turbulent Froude number and turbulent Reynolds number for DNS, laboratory experiments, and field measurements: +, towed grid experiments (Britter, 1985; Rehmann and Koseff, 2004; Rottman and Britter, 1986); ×, DNS (Stretch et al., 2010); ●, ocean thermocline (Yamazaki, 1990); ▲, inflow to stratified tidal channel (Gargett et al., 1984). Other sources: [1]Imberger and Ivey (1991) and [2]Stacey et al. (1999). The dashed line indicates the range of parameters for measurements in the thermocline of a lake (Saggio and Imberger, 2001), and the dotted lines show contours of Grashof number.[10]

high Froude numbers in others indicate the importance of inertia and help to explain the differences between RDT and observations (see previous section). The low Froude number for thermals either falling in weak stratification or impinging on a thermocline (Imberger and Ivey, 1991) may be suitable for RDT, but the large Reynolds numbers might decrease its accuracy. While most of the measurements of Saggio and Imberger (2001) in the thermocline of Lake Kinneret have $Fr \approx 1$, some fall in the range of parameters most suitable for RDT. Similar observations apply to flow in a strongly stratified estuary (Etemad-Shahidi and Imberger, 2002) and flow in an estuarine embayment (Stevens, 2003). Applying RDT to a larger range of flows would require including the effects of the neglected nonlinear terms.

[10] Matlab code used to generate figure: RfPaperPlot2.m

Conclusions

Rapid distortion theory was used to compute mixing efficiencies for an unsheared homogeneous flow stratified by one or two active scalars. For a flow stratified by one scalar, mixing efficiencies increase with *Gr* up to a maximum value and they decrease as *Sc* increases. Rapid distortion theory predicts maximum mixing efficiencies of approximately 30% for low *Sc*, similar to results from DNS (Stretch et al., 2010), while maximum efficiencies of 6% for heated water are similar to those in laboratory experiments (Rehmann and Koseff, 2004). However, RDT underpredicts the maximum efficiency for saltwater and also the value of *Gr* at which the efficiency becomes constant. For flow stratified by two scalars, the mixing efficiency decreases as R_ρ decreases, as in experiments and semi-empirical models (Jackson and Rehmann, 2003a; Martin and Rehmann, 2006). Predictions agree with results from experiments best at higher R_ρ, while they fall below the measured mixing efficiencies at low R_ρ, when more of the density gradient is due to salinity. Although RDT is restricted to strongly stratified flows, it complements numerical simulations by allowing mixing efficiencies to be evaluated over a much larger range of Schmidt numbers and shows that results from DNS should be treated with caution when applied to lakes and oceans. Extending RDT to include nonlinear interactions should improve the agreement between the theory and observations and increase the usefulness of the theory.

CHAPTER 3: NONLINEAR INTERACTIONS IN STRATIFIED TURBULENCE

Introduction

Flows existing in the natural environment can exhibit a wide variety of different characteristics – from the permanent, weakly stratified conditions of Lake Baikal in Russia that result in weak mixing (Ravens et al., 2000) to the more stratified, energetic tidal channel in British Columbia where a significant amount of mixing takes place (Gargett and Moum, 1995). Regardless, it is not physically possible to obtain field measurements for each and every scenario and as a result models become a valuable tool to predict behaviors in turbulent flows. However, the stratified conditions present in many environmental flows lie somewhere in between the two extreme cases of strong or weak stratification. Established models exist for weakly stratified flows and also for strongly stratified flows, but it is expected that their predictions become less accurate as the flow becomes more moderately stratified. Here we investigate modifications to the existing rapid distortion theory (RDT) model to improve its use for flows that have more moderate stratification.

One way the degree of stratification can be quantified is through the Froude number *Fr*. Imberger and Ivey (1991) obtained field measurements from a variety of flow regimes seen in lakes (their Figure 3) and a wide range of *Fr* can be seen. While both large values (i.e., $Fr > 1$, weak stratification) and small values (i.e., $Fr < 1$, strong stratification) of *Fr* exist, many flows lie somewhere around $Fr \approx 1$, indicating a more moderate level of stratification. In general, eddy diffusivity and two-equation models are commonly used for weakly stratified turbulence and RDT is used when strong stratification is present (Figure 3.1). If RDT could be extended to better model more moderately stratified flows, its applicability for use in environmental flows would be greatly improved.

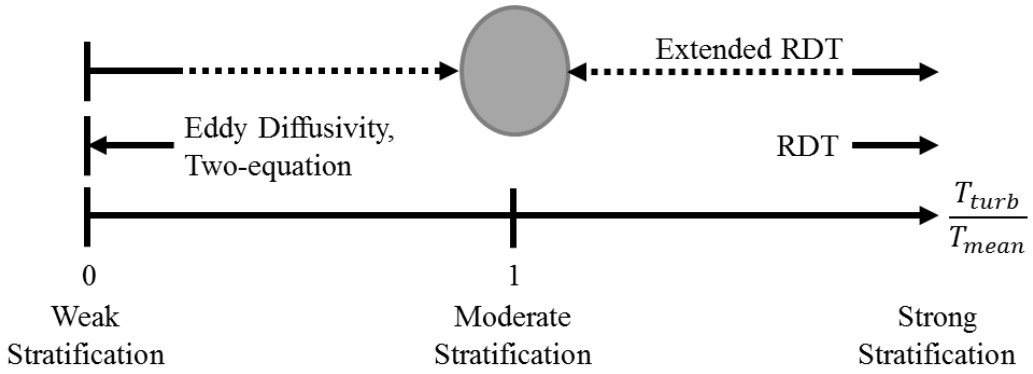

Figure 3.1: Commonly used turbulence models for given stratification conditions.[11]

In the turbulence models commonly used for weakly stratified flows, the Reynolds stress $-\overline{u_m' u_n'}$ present in the Reynolds-averaged conservation of momentum equation is related to a new parameter called the turbulent eddy viscosity ν_t through a gradient-transport approximation (e.g., $-\overline{u_1' u_3'} = \nu_t \, \partial u_1 / \partial x_3$) where primes denote fluctuating velocity components and the overbar indicates an ensemble average. This parameter is similar to the molecular viscosity of a fluid, but represents the turbulent nature of the flow and often holds a numerical value several orders of magnitude larger (Kundu and Cohen, 2008). In general, the eddy viscosity is composed of a velocity scale u_λ and length scale λ representative of the largest, energy containing eddies (i.e., $\nu_t = u_\lambda \lambda$). The eddy viscosity model simply specifies this value, whereas two-equation models go one step further by specifying an equation to solve for each term. Fundamentally, the concept of an eddy viscosity is physically flawed because the viscosity is treated as a property of the flow not of the fluid (Tennekes and Lumley, 1972), but nonetheless two-equation models have been shown to accurately predict geophysical flows (Mellor and Yamada, 1982). Also, both of these models require the unphysical situation of a negative diffusivity to get an upgradient flux and, as a result, cannot predict the restratification process that occurs in stratified flows.

Stratification can be found in water bodies such as oceans and lakes where density gradients are due to active scalars like salt, heat, or a combination of both. In this type of flow regime there are two time scales of interest, the mean flow time ($T_{mean} = N^{-1}$) and

[11] Figure location: ModelDiagram.pptx

turbulence time ($T_{turb} = \lambda / u_\lambda$), where *N* is the buoyancy frequency. Flows can be described as more strongly stratified when the ratio of these two time scales is large:

$$\frac{T_{turb}}{T_{mean}} = \frac{N\lambda}{u_\lambda} = \frac{1}{Fr} = Ri^{1/2} \gg 1 \tag{3.1}$$

where *Ri* is the Richardson number. As *Ri* increases, turbulence is suppressed along with the vertical transport of the active scalars (Kundu and Cohen, 2008). Rapid distortion theory can be used for strongly stratified flows in weak turbulence, and it can predict restratification (Jackson et al., 2005). The main assumption in RDT is that in strongly stratified flows an eddy is rapidly distorted by gravity before it has time to completely turn over or, in other words, the mean flow time is much shorter than the turbulence time scale and the nonlinear terms are neglected. As a result, an energy cascade does not develop and nonlinear interactions between eddies are not considered.

The governing equations for RDT originate from the conservation of mass, momentum, and buoyancy. The conservation equations are developed for the fluctuating quantities and are also linearized whereby the nonlinear terms (i.e., products of fluctuating terms) are neglected in order to reach closure. Negligible mean flow is also assumed. In Fourier representation, the governing equations are

$$\frac{d\hat{u}_j}{dt} = \left(\frac{k_j k_3}{k^2} - \delta_{j3} \right) \hat{b} - \nu k^2 \hat{u}_j \ , \tag{3.2}$$

$$\frac{d\hat{b}}{dt} = N^2 \hat{u}_3 - D k^2 \hat{b} \tag{3.3}$$

where hats denote the Fourier amplitude of the buoyancy and velocity u_j. The subscript *j* can hold the value of 1, 2, or 3 and indicates the directions *x*, *y*, and *z*, respectively. The above equations are also a function of time *t*, the wavenumber *k*, kinematic viscosity *v*, and molecular diffusivity *D*, and they also include the Kronecker delta δ_{j3} which is equal to one when $j = 3$ and zero when $j \neq 3$. Hanazaki and Hunt (1996) provide an analytical solution based on (3.2) and (3.3) that will be used in this work.

Turbulence is thought to be dominated by buoyancy forces at the large scale and dissipative, nonlinear processes at small scales (Lienhard and Van Atta, 1990, hereinafter

LVA; Kevlahan and Hunt, 1997, hereinafter KH). While many researchers acknowledge that nonlinear interactions can influence turbulence (Galmiche and Hunt, 2002; Liechtenstein et al., 2005), actually providing a quantitative expression for these neglected terms presents a significant theoretical, conceptual, and mathematical challenge. Isaza and Collins (2009) compared RDT and direct numerical simulations (DNS) for homogeneous shear flow and concluded that including a model for one of the nonlinear terms would improve the applicability of RDT at long times. The nonlinear term is composed of a random (i.e., stochastic) stirring term and a dampening term (Cambon and Scott, 1999), or in the case of strained flow, a 'slow' term which refers to nonlinear contributions at long times (Cambon and Scott, 1999; Isaza and Collins, 2009). Several stochastic closure models such as direct interaction approximation (DIA), Lagrangian history direct interaction (LHDI), eddy damped quasi-normal Markovian (EDQNM), or the test field model (TFM) attempt to resolve the nonlinearity instead of just completely neglecting the term, but these models are cumbersome and not frequently used (Graebel, 2007; Chapter 10). Some examples of stochastic model applications include work by Herring and Kerr (1993) to compare DNS to DIA and TFM in an attempt to better understand turbulence structure, Gotoh et al. (1993) who used DNS and DIA to compute turbulent diffusion for homogeneous, isotropic turbulence, and Cambon et al. (1997) who used EDQNM to evaluate nonlinear effects in homogenous rotating turbulence. Stochastic closure models like EDQNM use various applications of Green's functions which describe the time evolution of turbulence (Cambon and Scott, 1999). Although these models are closed, there are several shortcomings: they do not capture the intermittency of turbulence, nonlinearities are overestimated, and turbulent structures (e.g., sheets, filaments, etc.) are not predicted (Frisch, 1995; Chapter 9). Other closure models, including renormalization group (RNG) analysis (Frisch, 1995; Chapter 9) and nonlinear mapping of fields (Kraichnan, 1991), are thought to potentially provide insight to the energy cascade and intermittency questions, respectively. One of the simplest closure models for turbulence represents the nonlinear term by an eddy viscosity. Use of an eddy viscosity to close RDT has been shown to predict kinetic energy variations in rotating sheared flow that agree with large eddy simulations (Cambon and Scott, 1999), but no application to stratified flows has been identified. Given this history of closure models, the work by KH takes on a

different perspective in that they provide an analytical expression for the nonlinear terms neglected from RDT.

The research completed by KH works to gain a better understanding of the inherent limitations of RDT in its linear form for turbulence with strong irrotational straining. Through the addition of mathematical expressions for nonlinear terms to the linear RDT equations, KH discuss time scales for which RDT is valid and consequently when nonlinear interactions become important. Several scenarios were analyzed to provide more precise time frame definitions of when RDT is valid including the inviscid range, and more specifically possible contributions from 'local' and 'global' nonlinear sources, and the viscous range. Local nonlinear sources are described by the wavespace range from zero to some arbitrary transition value ζ and global contributions make up the remaining wavespace range from ζ to infinity (KH). The transition value lies between $e^{-\Gamma t}$ and one, where Γ is the strain rate. Further evaluation yields that the fastest growing nonlinear terms are those associated with advection (KH). Usage of the nonlinear expressions developed by KH for purposes of actually evaluating turbulence was not found. Several publications citing KH pertained specifically to strained flows and used the work by KH to confirm that the use of linear RDT was valid (Ayyalasomayajula and Warhaft, 2006; Godeferd et al., 2001; Teixeira, 2011). Other citations of KH reference their conclusion that straining motion prevents the formation of nonlinear motions and produces sheet-like turbulence structures rather than tube-like ones (Brethouwer et al., 2003; Elsinga and Marusic, 2010; Hunt et al., 2001).

We use a numerical model for unsheared homogeneous turbulence in a stratified fluid and compare the results to experimental data from thermally stratified wind tunnel experiments. Initial investigations of RDT modifications and extensions using eddy diffusivity and two-equation model techniques are discussed in the Initial Investigations section. Mathematical expressions, using an approach similar to KH, for nonlinear terms relevant to stratified flows are derived and a model system of equations are developed and evaluated in the next section. To conclude, a summary of the main findings and recommendations for future work will be presented.

Initial Investigations

Wind tunnel experiments completed by LVA and Yoon and Warhaft (1990, hereinafter YW) provide valuable documentation of turbulence measurements for thermally stratified flows. These experiments were completed for a series of different levels of stratification (i.e., series of different *Fr* values) and measurements were recorded at various stations throughout the wind tunnel. While several experiments have been completed in salt stratified water (Schmidt number *Sc* = 700), detailed measurements are easier to obtain for heated air (*Sc* = 0.7). Air tunnel experiments can reach larger temperature gradients (YW) and result in a steadier temperature profile (LVA). Because temperature in air has a larger molecular diffusivity than salt in water, the scalar field can be resolved more accurately and restratification is more clearly seen (LVA). The presence of a grid used to generate the turbulence inherently creates internal waves; however, wind tunnels can be designed to prevent this phenomenon (LVA). Both LVA and YW were able to show quantitatively that no internal waves were present by evaluating phase measurements between the vertical velocity and temperature.

Even though experiments completed by LVA and YW are both described as strongly stratified flows, differences exist between them (Figure 3.2). Both had approximately the same Reynolds number *Re* range, but the LVA experiments were completed at lower *Fr* (i.e., stronger stratification), where *U* is the mean velocity of the air flow and *M* is size of the mesh grid, respectively, used to generate the turbulence in the experiments. As a result of the stronger stratification in LVA experiments, buoyancy began to affect the turbulence much closer to the grid used to generate the turbulence (YW). In addition, the LVA experiments had higher initial temperature fluctuations than those completed by YW resulting in differences between the initial conditions. Stratified flows are highly sensitive to initial conditions (see Appendix B) and this difference is thought to be the reason why no upgradient fluxes appear in the LVA data even though they are actually more strongly stratified (YW). Experiments completed by YW span a wider range of stratification levels, from completely unstratified (i.e., the passive case) to a level slightly below that investigated by LVA, and therefore capture a more moderate degree of stratification. An upgradient flux appears for only the strongest degree of stratification evaluated by YW, as would be expected

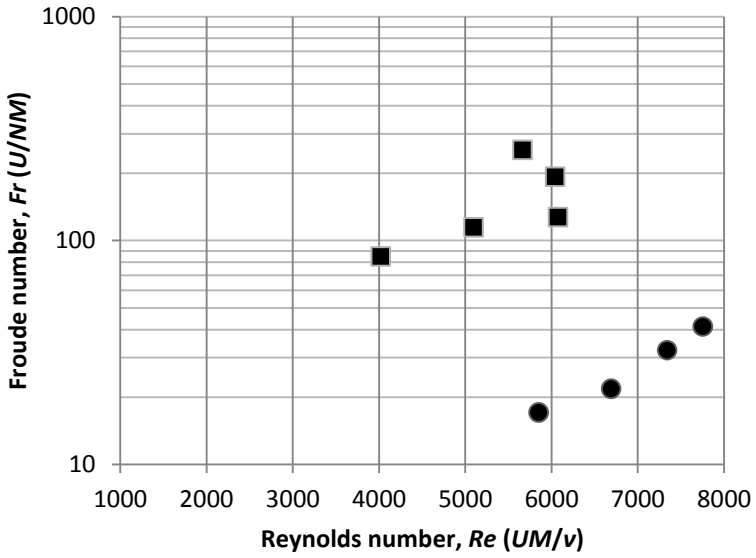

Figure 3.2: Characteristics of YW (■) and LVA (●) experiments for $Sc = 0.7$.[12]

when there are minimal initial temperature fluctuations. Regardless of the stratification strength, fluxes align up until a certain point before either restratifying or remaining downgradient (YW). YW acknowledge this behavior but do not draw any conclusions about what parameter or mechanism may cause an upgradient flux to occur or not.

Investigations into the behavior of stratified flows have also been completed using another approach. Gerz and Yamazaki (1993) used DNS to evaluate turbulence generated from temperature differences, similar to what is seen in the ocean thermocline. The simulations were completed for low Sc at $Re \approx 60$ over a range of stratification numbers. The stratification number is related to the density gradient and used to describe the flow regime: When stratification numbers are greater than one turbulence is present and nonlinear interactions are considered to be small, whereas for stratification numbers less than one the flow is dominated by nonlinear interactions which cause large decay of the vertical heat flux over time (Gerz and Yamazaki, 1993). The vertical flux correlation coefficient curves presented by Gerz and Yamazaki (1993) show the oscillating pattern between mixing and restratification that occurs in stratified flows and also the decay of turbulence over time (their Figure 8).

[12] Figure location: Experimental Data Comparison.xlsx

To begin, we focus on the experiments of LVA and YW and compare the results to the original RDT model with nonlinear terms neglected (Figure 3.3). Three dimensionless parameters are required for input to RDT to generate vertical flux correlation coefficient curves: the Grashof number Gr which is a ratio of the buoyant to viscous forces, r which is the ratio of initial potential energy PE_0 to initial kinetic energy KE_0, and Sc. The vertical flux correlation coefficient $R_{\rho w}$, which describes the correlation between the vertical velocity fluctuation and the density fluctuation, oscillates and decays over dimensionless time τ, similar to behavior shown by Gerz and Yamazaki (1993). The magnitude and period length of the correlation curve produced by RDT agree quite well with the most strongly stratified YW dataset (Fr = 84.8) with exception of the peak timing. When using the same RDT model and comparing to the LVA data there is agreement at early times, but shortly thereafter both the peak timing and magnitude begin to differ. This lack of agreement could possibly be due to differences between model and experiment initial conditions. One goal of the extended model is to predict the lack of upgradient fluxes at large times (i.e., peak vertical flux correlation coefficient magnitude of approximately zero), as this particular behavior is represented in both experiments. Another goal of the extended model is to understand what parameter influences the period so better peak timing can be reached at larger times since the timing of the second peak is different for both data sets.

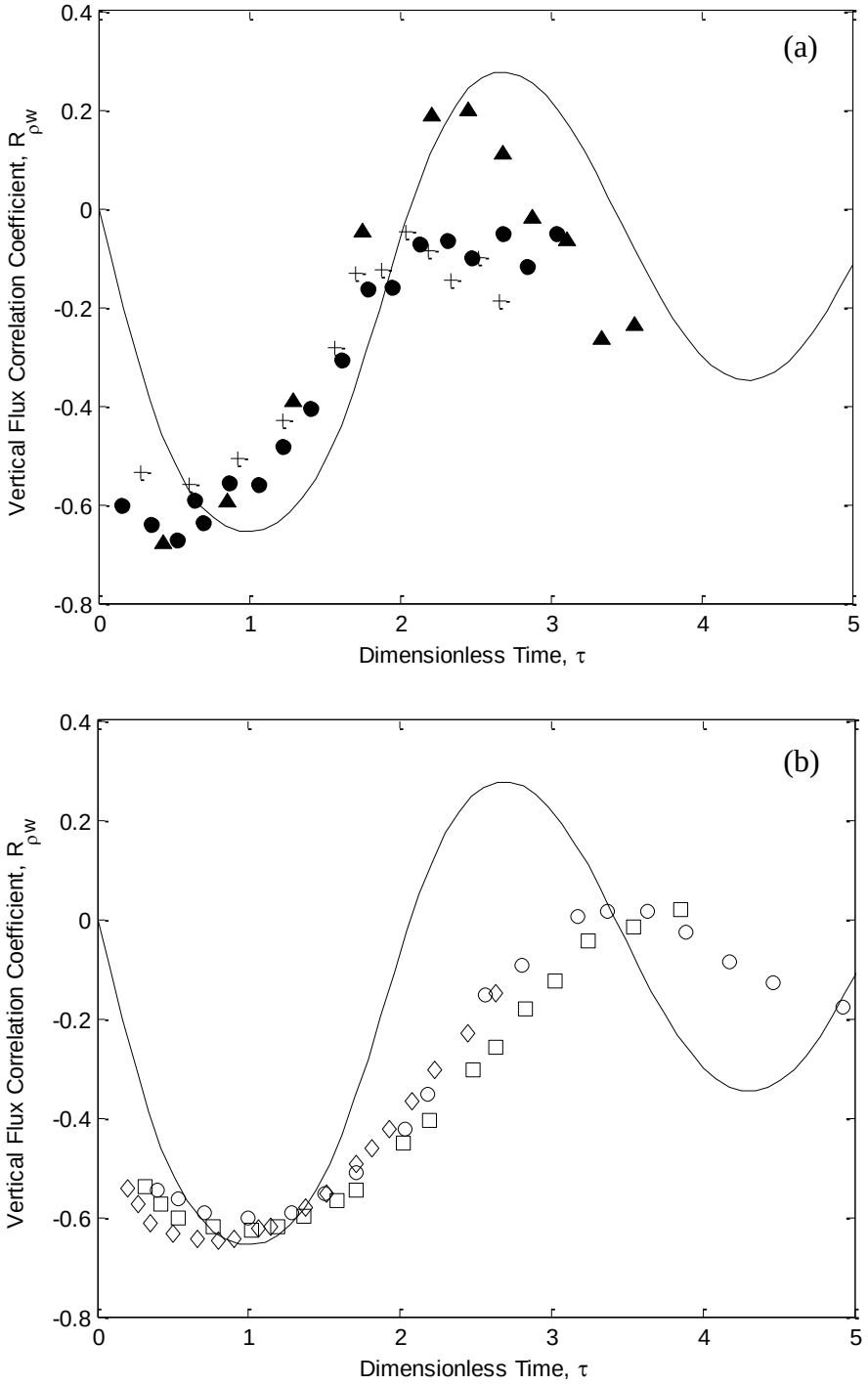

Figure 3.3: Comparison of RDT to experimental results: (a) YW (▲, *Fr* = 84.8; ●, *Fr* = 114; +, *Fr* = 127) to RDT (–, *Gr* = 1.25, *r* = 1.35 and *Sc* = 0.7) and (b) LVA (○, *Fr* = 17.1; □, *Fr* = 21.8; ◊, *Fr* = 32.4) to RDT (–, *Gr* = 2.25 and *r* = 1.26 and *Sc* = 0.7). [13]

[13] Matlab code used to generate figure: (a) hhanalytical.m (b) lva.m

Several unsuccessful extensions to RDT were made in an attempt to better reflect the experimental data. The attempts here make comparisons to the LVA experimental data primarily due to its availability. More detailed explanations regarding the different extension attempts and figures comparing the attempted models and experimental data can be found in Appendix B.

- *Modification of RDT input parameters*

  For a given Schmidt number two additional parameters are required to be input to the RDT model: the Grashof number and the initial energy ratio. Various combinations of these parameters were investigated and the approximate magnitude and timing of either the first or second peak of the correlation coefficient curve could be predicted, but not both simultaneously.

- *Varying turbulent eddy diffusivity*

  An equation relating the turbulent eddy diffusivity D_T and time was established using LVA data. The relationship was then used to redefine the *Gr* input into the RDT model. Use of a varying diffusivity moves the correlation coefficient curve vertically to align better at earlier times, but does not reflect LVA data at long times where both peak timing and magnitude discrepancies exist.

- *Diffusivity simulations*

  In an attempt to account for variations in the turbulent eddy diffusivity that may be a function of both the wavenumber and time, a new vertical density flux was computed numerically for each time step of the RDT model. Then, this unique value of the vertical density flux was then used to calculate a new turbulent eddy diffusivity for each time step. Predictions using this approach more closely match the original RDT solution for early times than the LVA data and results in a worse prediction of the correlation coefficient curve at large times.

- *k-ε model*

  Moving away from RDT, briefly, the vertical density flux plotted as a function of time was predicted using the *k-ε* model (where *k* in this case stands for the turbulent kinetic energy, not wavenumber) and compared to LVA data. The magnitude of both curves lie

within the same general range and the overall decreasing trend of the data is similar, but the *k*-ε model does not accurately represent the trend of the measured data points.

- *Diffusivity simulations with k-ε model*

  Combining the strategy of the diffusivity simulation with the *k*-ε model, a simulation is performed where the turbulent eddy viscosity (and ultimately the turbulent eddy diffusivity through use of *Sc*) is determined by multiplication of a length scale and a velocity scale. Again, this output more closely matches the trend of the original RDT and still does not reflect LVA data at large times.

Given the approaches tried thus far, none of them reflect the observed behavior of the vertical flux correlation coefficient curve after approximately $\tau = 1.5$ and in fact, many predict magnitude differences greater than that of the original RDT model. In order to more appropriately reflect a moderately stratified flow, the correlation coefficient curve would need to have a longer period and faster decay (i.e., smaller amplitude at larger times) which would result in better alignment with the peak timing of measured data for this condition. In stratified turbulence, dissipative effects become important at smaller scales which correspond to larger wavelengths (LVA). One aspect that we have not yet considered is accounting for non-local interactions between scales. At more moderate levels of stratification it is plausible that nonlinear effects become relevant at an earlier time, which may be why RDT has difficulty predicting the flux behavior for this type of flow.

Addition of Nonlinear Term to RDT for Stratified Flow

Instead of analyzing turbulence with strong irrotational straining, we attempt to apply the approach taken by KH to turbulence with strong stratification. KH begin with the equations of conservation of mass and conservation of vorticity and present Fourier representations of vorticity ω_j and velocity u_j. Substitution of the Fourier representations into the conservation of vorticity equation yields an equation for the evolution of $\hat{\omega}_j$ with respect to time and is composed of both linear and nonlinear terms. This 'new' RDT equation is then made dimensionless and scaled for long-time solutions by assuming $\Gamma t >> 1$. Under this assumption, the zeroth-order solution is reached by neglecting the nonlinear terms and applying an integrating factor. Continuing with the perturbation method, the first order

correction is made through the addition of the largest nonlinear terms. The nonlinear term is made up of several convolutions and only terms of the order $e^{-\Gamma t}$ and larger are included. Computing the convolutions leads to expressions for the nonlinear terms.[14] KH go on to evaluate the asymptotic behavior of the nonlinear integrals for turbulence scales in the inviscid range and discuss time frames of when the linear and nonlinear RDT solutions are valid for this flow.

Our evaluation of stratified flows using RDT begins with equations for the conservation of mass, momentum, and buoyancy written in Einstein index notation where *m* and *n* are indices:

$$\frac{\partial u_m'}{\partial x_m} = 0\,, \tag{3.4}$$

$$\underset{1}{\frac{\partial u_m'}{\partial t}} + \underset{2}{U_n \frac{\partial u_m'}{\partial x_n}} = \underset{3}{-u_n' \frac{\partial U_m}{\partial x_n}} - \underset{4}{\frac{\partial}{\partial x_n}(u_m' u_n')} + \underset{5}{\frac{\partial}{\partial x_n}(\overline{u_m' u_n'})} - \underset{6}{\frac{1}{\rho_0}\frac{\partial p'}{\partial x_m}} - \underset{7}{b'\delta_{m3}} + \underset{8}{\nu \frac{\partial^2 u_m'}{\partial x_n^2}}\,, \tag{3.5}$$

$$\underset{1}{\frac{\partial b'}{\partial t}} + \underset{2}{U_n \frac{\partial b'}{\partial x_n}} = \underset{3}{-\frac{g}{\rho_0} u_n' \frac{\partial \rho'}{\partial x_n}} - \underset{4}{\frac{\partial}{\partial x_n}(b' u_n')} + \underset{5}{\frac{\partial}{\partial x_n}(\overline{b' u_n'})} + \underset{6}{D \frac{\partial^2 b'}{\partial x_n^2}} \tag{3.6}$$

where primes (') denote fluctuating quantities of buoyancy and velocity. The mean flow velocity U_m, as well as most other quantities in the above equations, vary with respect to the spatial coordinate x_n where n =1, 2, 3 corresponds to the directions x, y, and z, respectively. The remaining terms include the density ρ, reference density ρ_0, pressure p, and the acceleration due to gravity g. Assuming there is negligible mean flow and that the turbulence is homogeneous, terms 2, 3, and 5 can be neglected from (3.5) and terms 2 and 5 neglected from (3.6). In the typical application of RDT, the momentum and buoyancy equations are linearized (i.e., term 4 in (3.5) and in (3.6) are neglected). However, since the purpose of this work is to evaluate the effect of nonlinear interactions they will remain.

We must also consider the Poisson equation for the pressure fluctuation for future use in developing the Fourier coefficient equations:

[14] There appear to be a few discrepancies between the nonlinear terms presented in KH (1997) (their equations 3.2a and 3.2b) and the set on nonlinear terms we arrived at using their approach. There are a couple of sign differences, a wavenumber vector that should be in shifted form from the convolution, and several terms of appropriate order that are not included.

$$-\frac{1}{\rho_0}\frac{\partial^2 p'}{\partial x_m{}^2} = \frac{\partial u_n'}{\partial x_m}\frac{\partial u_m'}{\partial x_n} + \frac{\partial b'}{\partial x_3} \tag{3.7}$$

where x_3 indicates the vertical direction. The Poisson equation is obtained by applying $\partial/\partial x_m$ to the momentum equation (3.5) and using conservation of mass.

The first step in obtaining the Fourier coefficient equations is to apply the Fourier transform,

$$F'(\mathbf{x},t) = \int_{\mathbf{k}} \hat{F}(\mathbf{k},t) e^{i\mathbf{k}\cdot\mathbf{x}} d\mathbf{k}\,, \tag{3.8}$$

where $i = \sqrt{-1}$, to each term in the Poisson equation (3.7) , momentum (3.5), and buoyancy (3.6) equations. The Fourier transform converts an arbitrary fluctuating function F' as a function of **x**, a vector that refers to a coordinate system that follows the mean flow, to a function of **k**, a wavenumber vector with three components:

$$k_1 = k\sin\theta\cos\phi\,,\ k_2 = k\sin\theta\sin\phi \text{ and } k_3 = k\cos\theta\,. \tag{3.9}$$

The corresponding directions and angles are shown in Figure 3.4 where θ is the angle between the wavenumber vector and the vertical and ϕ lies in the horizontal plane. Recall that the dot product of the two vectors present in the exponent is equivalent to $k_m x_m$.

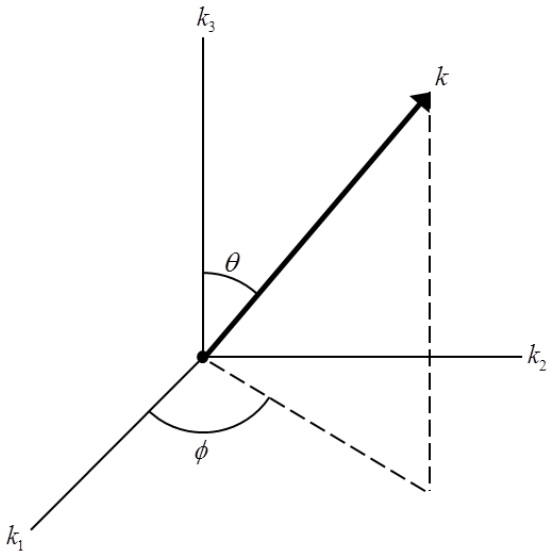

Figure 3.4: Components of wavenumber vector.[15]

[15] Figure location: CoordSystemDiagram.pptx

After applying the Fourier transform to each term in the Poisson equation and simplifying though a series of steps, the following relationship is reached:

$$\frac{\hat{p}}{\rho} = \frac{ik_3\hat{b}}{k^2} - \frac{k_m\hat{u}_j * k_j\hat{u}_m}{k^2} = \frac{ik_3\hat{b}}{k^2} - \hat{P} \tag{3.10}$$

where the convolution ($*$) can be defined by the product of an arbitrary pair of functions *F* and *G* shifted across some range of wavenumbers

$$(F * G)(k) = (G * F)(k) = \int F(k')G(k-k')dk' . \tag{3.11}$$

Once the Fourier transform has been applied to each term in the momentum equation, the Poisson expression (3.10), which is a function of $\hat{u}$, $\hat{b}$, and *k*, can be substituted into the momentum equation to eliminate the pressure term. Using similar techniques as those to simplify the Poisson equation, the resulting momentum and buoyancy equations are:

$$\frac{\partial\hat{u}_m}{\partial t} = \left(\frac{k_m k_3}{k^2} - \delta_{m3}\right)\hat{b} - \nu k^2\hat{u}_m - ik_m\hat{P} + ik_n\hat{u}_n * \hat{u}_m , \tag{3.12}$$

$$\frac{\partial\hat{b}}{\partial t} = N^2\hat{u}_3 - Dk^2\hat{b} - i(k_n\hat{b} * \hat{u}_n) . \tag{3.13}$$

These equations are identical to the typical governing RDT equations (3.2) and (3.3) except for the presence of three additional terms resulting from the nonlinearity. The above equations are made dimensionless by

$$\hat{u}'_m = \frac{\hat{u}_m}{u_0},\ \hat{b}' = \frac{\hat{b}}{Nu_0},\ \kappa = kL \text{ and } t' = \frac{tu_0}{L_0} \tag{3.14}$$

where u_0 and L_0 are the velocity and length scales of the largest eddies, κ is the dimensionless wavenumber, and t' is dimensionless eddy turnover time. These variables also combine to form more commonly recognized dimensionless parameters, namely the Froude number, Reynolds number, and Péclet number *Pe*:

$$Fr = \frac{u_0}{NL},\ Re = \frac{u_0 L_0}{\nu} \text{ and } Pe = \frac{u_0 L_0}{D} . \tag{3.15}$$

As in KH, we consider dimensionless time τ at long times since that is when nonlinear terms are anticipated to influence the turbulence evolution. We do this by setting

$$\tau = \frac{t'}{Fr} = \frac{tu_0}{L_0}\frac{NL_0}{u_0} = Nt . \tag{3.16}$$

After applying the above series of definitions (and dropping the prime notation), the dimensionless governing equations for RDT including the presence of nonlinear interactions are:

$$\frac{d\hat{u}_j}{d\tau} = \left(\frac{\kappa_j \kappa_3}{\kappa^2} - \delta_{j3} \right) \hat{b} - \frac{Fr}{Re} \hat{u}_j \kappa^2 + Fr \hat{M}_j , \tag{3.17}$$

$$\frac{d\hat{b}}{d\tau} = \hat{u}_3 - \frac{Fr}{Pe} \hat{b} \kappa^2 - Fr \hat{B} , \tag{3.18}$$

$$\hat{M}_j = i \left[\frac{\kappa_j}{\kappa^2} \left(\kappa_n \hat{u}_m * \kappa_m \hat{u}_n \right) - \kappa_n \hat{u}_j * \hat{u}_n \right] , \tag{3.19}$$

$$\hat{B} = i \left(\kappa_j \hat{b} * \hat{u}_j \right) \tag{3.20}$$

where the $\hat{M}_j$ and $\hat{B}$ expressions account for the nonlinear advection. The nonlinear terms have an appearance similar to that presented by KH (their equation (2.8)) in that a set of convolutions is present.

The governing equations now need to be solved for the Fourier amplitudes $\hat{u}_j$ and $\hat{b}$. We evaluate these equations first for a flow with *Sc* equal to 1 (i.e., $\nu = D$ and therefore, $Re = Pe$) at the first order $O(1)$ whereby the nonlinear terms are initially neglected similar to the governing RDT equations presented in Hanazaki and Hunt (1996). In this case, the terms dependent on the buoyant and viscous forces (i.e., $Fr/Re = Gr^{-1}$) can be removed by multiplying (3.17) and (3.18) by an integrating factor of exp ($Gr^{-1}\kappa^2\tau$). If two new variables, $\hat{r}_j$ and $\hat{s}$, are defined by

$$\hat{u}_j = \hat{r}_j e^{-Gr^{-1}\kappa^2\tau} , \tag{3.21}$$

$$\hat{b} = \hat{s} e^{-Gr^{-1}\kappa^2\tau} \tag{3.22}$$

then (3.17) and (3.18) become

$$\frac{d\hat{r}_j}{d\tau} = \left(\frac{\kappa_j \kappa_3}{\kappa^2} - \delta_{j3} \right) \hat{s} , \tag{3.23}$$

$$\frac{d\hat{s}}{d\tau} = \hat{r}_3 . \tag{3.24}$$

Once $\hat{r}_j$ and $\hat{s}$ are computed, then $\hat{u}_j$ and $\hat{b}$ can be determined from (3.21) and (3.22). A linear system of equations can be solved by trying solutions of the form

$$\hat{r}_j \propto e^{\sigma\tau} \ , \tag{3.25}$$

$$\hat{s} \propto e^{\sigma\tau} \tag{3.26}$$

and in matrix form:

$$\begin{bmatrix} \sigma & 0 & 0 & -\kappa_1\kappa_3/\kappa^2 \\ 0 & \sigma & 0 & -\kappa_2\kappa_3/\kappa^2 \\ 0 & 0 & \sigma & 1-\kappa_3^2/\kappa^2 \\ 0 & 0 & -1 & \sigma \end{bmatrix} \begin{bmatrix} \hat{r}_1 \\ \hat{r}_2 \\ \hat{r}_3 \\ \hat{s} \end{bmatrix} = \begin{bmatrix} 0 \\ 0 \\ 0 \\ 0 \end{bmatrix} . \tag{3.27}$$

The system (3.27) has a non-zero solution only if

$$\sigma^2 \left[\sigma^2 + \left(1 - \frac{\kappa_3^2}{\kappa^2} \right) \right] = 0 \tag{3.28}$$

with four roots, or eigenvalues, of $\sigma = 0, 0, +iw$ and $-iw$ where

$$w = \left(1 - \frac{\kappa_3^2}{\kappa^2} \right)^{1/2} . \tag{3.29}$$

Thus, using the forms (3.25) and (3.26) combined with the trigonometric definitions

$$\cos(w\tau) = \frac{e^{iw\tau} + e^{-iw\tau}}{2} \ \text{ and } \ \sin(w\tau) = \frac{e^{iw\tau} - e^{-iw\tau}}{2i} \tag{3.30}$$

the solution of equations for (3.23) and (3.24) is

$$\hat{r}_1 = A_1 + A_2 \cos(w\tau) + A_3 \sin(w\tau) , \tag{3.31}$$

$$\hat{r}_2 = B_1 + B_2 \cos(w\tau) + B_3 \sin(w\tau) , \tag{3.32}$$

$$\hat{r}_3 = C_1 + C_2 \cos(w\tau) + C_3 \sin(w\tau) , \tag{3.33}$$

$$\hat{s} = D_1 + D_2 \cos(w\tau) + D_3 \sin(w\tau) . \tag{3.34}$$

The coefficients, or eigenvectors A_j, B_j, C_j, and D_j, in the above equations can be determined by relating them to each other by either substituting (3.31)–(3.34) to (3.23) and (3.24) or applying initial conditions (i.e., set $\tau = 0$) to (3.21) and (3.22). Equation (3.23) for j = 1 gives

$$A_2 = -\frac{1}{w}\frac{\kappa_1\kappa_3}{\kappa^2}D_3, \tag{3.35}$$

$$A_3 = \frac{1}{w}\frac{\kappa_1\kappa_3}{\kappa^2}D_2, \tag{3.36}$$

$$D_1 = 0, \tag{3.37}$$

and (3.23) for $j = 2$ yields

$$B_2 = -\frac{1}{w}\frac{\kappa_2\kappa_3}{\kappa^2}D_3, \tag{3.38}$$

$$B_3 = \frac{1}{w}\frac{\kappa_2\kappa_3}{\kappa^2}D_2. \tag{3.39}$$

Equation (3.24) results in

$$C_1 = 0, \tag{3.40}$$

$$C_2 = wD_3, \tag{3.41}$$

$$C_3 = wD_2. \tag{3.42}$$

Applying the initial conditions gives

$$\hat{u}_1(\underline{\kappa},0) = A_1 - \frac{1}{w^2}\frac{\kappa_1\kappa_3}{\kappa^2}C_2, \tag{3.43}$$

$$\hat{u}_2(\underline{\kappa},0) = B_1 - \frac{1}{w^2}\frac{\kappa_2\kappa_3}{\kappa^2}C_2, \tag{3.44}$$

$$\hat{u}_3(\underline{\kappa},0) = C_2, \tag{3.45}$$

$$\hat{b}(\underline{\kappa},0) = D_2. \tag{3.46}$$

Inserting the constants from (3.37)–(3.46) into the solution of equations (3.31)–(3.34) and then into the relationship defined by (3.21) and (3.22) the $O(1)$ general solution for the Fourier coefficients is

$$\hat{u}_1(\underline{\kappa},\tau) = e^{-Gr^{-1}\kappa^2\tau}\left\{\hat{u}_1(\underline{\kappa},0) + \hat{u}_3(\underline{\kappa},0)\frac{\kappa_1\kappa_3}{\kappa^2}\frac{1}{w^2}\left[1-\cos(w\tau)\right] + \hat{b}(\underline{\kappa},0)\frac{\kappa_1\kappa_3}{\kappa^2}\frac{1}{w}\sin(w\tau)\right\}, \tag{3.47}$$

$$\hat{u}_2(\underline{\kappa},\tau) = e^{-Gr^{-1}\kappa^2\tau}\left\{\hat{u}_2(\underline{\kappa},0) + \hat{u}_3(\underline{\kappa},0)\frac{\kappa_2\kappa_3}{\kappa^2}\frac{1}{w^2}\left[1-\cos(w\tau)\right] + \hat{b}(\underline{\kappa},0)\frac{\kappa_2\kappa_3}{\kappa^2}\frac{1}{w}\sin(w\tau)\right\}, \tag{3.48}$$

$$\hat{u}_3(\underline{\kappa},0) = e^{-Gr^{-1}\kappa^2\tau}\left[\hat{u}_3(\underline{\kappa},0)\cos(w\tau) - \hat{b}(\underline{\kappa},0)w\sin(w\tau)\right], \tag{3.49}$$

$$\hat{b}(\underline{\kappa},0) = e^{-Gr^{-1}\kappa^2\tau}\left[\hat{u}_3(\underline{\kappa},0)\frac{1}{w}\sin(w\tau) + \hat{b}(\underline{\kappa},0)\cos(w\tau)\right]. \tag{3.50}$$

If there is no initial velocity field, then terms with $\hat{u}_1(\underline{\kappa},0)$, $\hat{u}_2(\underline{\kappa},0)$ or $\hat{u}_3(\underline{\kappa},0)$ present will be neglected from (3.47)–(3.50). We will proceed under this assumption.

Now that an *O*(1) solution has been obtained, the long-time behavior of the nonlinear terms can be evaluated. We will start with nonlinear term $\hat{B}$ which corresponds to the buoyancy equation, see (3.20), and expand the repeated indices to

$$\hat{B} = i\kappa_1\hat{b} * \hat{u}_1 + i\kappa_2\hat{b} * \hat{u}_2 + i\kappa_3\hat{b} * \hat{u}_3. \tag{3.51}$$

The three individual terms that make up $\hat{B}$ will be evaluated individually and be identified by $\hat{B}_1$, $\hat{B}_2$, and $\hat{B}_3$ where subscripts 1, 2, and 3 indicate the first, second, and third terms on the right hand side of (3.51). Each term is solved for by inserting the respective Fourier coefficient expressions from the *O*(1) solution, completing the convolution, and simplifying through use of the trigonometric identities. The components of $\hat{B}$ are as follows, including evaluation over all wavespace per definition of the Fourier transform:

$$\hat{B}_1 = i\frac{1}{2}e^{-Gr^{-1}\kappa^2\tau}\int_0^{2\pi}\int_0^{\pi}\int_0^{\infty}\hat{b}(\underline{\kappa},0)\hat{b}(\underline{\kappa}-\underline{\kappa}',0)\kappa'^3 e^{2Gr^{-1}(\kappa\kappa'-\kappa'^2)\tau}\sin^2\theta' \times\cos\phi'\frac{(\kappa_1-\kappa_1')(\kappa_3-\kappa_3')}{(\kappa-\kappa')^2}\frac{1}{w''} \times\left(\sin\left[(w''+w')\tau\right]+\sin\left[(w''-w')\tau\right]\right)d\kappa' d\theta' d\phi', \tag{3.52}$$

$$\hat{B}_2 = i\frac{1}{2}e^{-Gr^{-1}\kappa^2\tau}\int_0^{2\pi}\int_0^{\pi}\int_0^{\infty}\hat{b}(\underline{\kappa},0)\hat{b}(\underline{\kappa}-\underline{\kappa}',0)\kappa'^3 e^{2Gr^{-1}(\kappa\kappa'-\kappa'^2)\tau}\sin^2\theta' \times\sin\phi'\frac{(\kappa_2-\kappa_2')(\kappa_3-\kappa_3')}{(\kappa-\kappa')^2}\frac{1}{w''} \times\left(\sin\left[(w''+w')\tau\right]+\sin\left[(w''-w')\tau\right]\right)d\kappa' d\theta' d\phi', \tag{3.53}$$

$$\hat{B}_3 = -i\frac{1}{4}e^{-Gr^{-1}\kappa^2\tau}\int_0^{2\pi}\int_0^{\pi}\int_0^{\infty}\hat{b}(\underline{\kappa},0)\hat{b}(\underline{\kappa}-\underline{\kappa}',0)\kappa'^3 e^{2Gr^{-1}(\kappa\kappa'-\kappa'^2)\tau}\sin 2\theta' w'' \times\left(\sin\left[(w''+w')\tau\right]+\sin\left[(w''-w')\tau\right]\right)d\kappa' d\theta' d\phi' \tag{3.54}$$

where

$$w' = \left(1-\frac{\kappa_3'^2}{\kappa'^2}\right)^{1/2} = \sin\theta' \ , \tag{3.55}$$

$$w'' = \left(1-\frac{(\kappa_3-\kappa_3')^2}{(\kappa-\kappa')^2}\right)^{1/2} = \left(1-\frac{(\kappa\cos\theta-\kappa'\cos\theta')^2}{(\kappa-\kappa')^2}\right)^{1/2} . \tag{3.56}$$

and the prime and double prime notation distinguishes between the unshifted and shifted terms from the application of the convolution. Altogether,

$$\hat{B} = ie^{-Gr^{-1}\kappa^2\tau}\int_0^{2\pi}\int_0^{\pi}\int_0^{\infty}\hat{b}(\underline{\kappa},0)\hat{b}(\underline{\kappa}-\underline{\kappa}',0)\kappa'^3 e^{2Gr^{-1}(\kappa\kappa'-\kappa'^2)\tau} \times\frac{1}{2w''}\left(\sin^2\theta'\cos\phi'\frac{(\kappa_1-\kappa_1')(\kappa_3-\kappa_3')}{(\kappa-\kappa')^2} + \sin^2\theta'\sin\phi'\frac{(\kappa_2-\kappa_2')(\kappa_3-\kappa_3')}{(\kappa-\kappa')^2} - \frac{w''^2}{2}\sin 2\theta'\right) \times\left(\sin\left[(w''+w')\tau\right]+\sin\left[(w''-w')\tau\right]\right)d\kappa' d\theta' d\phi'. \tag{3.57}$$

Alternatively, if no initial buoyancy field is considered, then terms including $\hat{b}(\underline{\kappa},0)$ will be neglected from the equations (3.47)–(3.50) and terms with $\hat{u}_1(\underline{\kappa},0)$, $\hat{u}_2(\underline{\kappa},0)$ or $\hat{u}_3(\underline{\kappa},0)$ will remain. For this case, the nonlinear term associated with the buoyancy equation will be of the form:

$$\hat{B} = ie^{-Gr^{-1}\kappa^2\tau}\int_0^{2\pi}\int_0^{\pi}\int_0^{\infty}\hat{u}_3(\underline{\kappa},0)\kappa'^3 e^{2Gr^{-1}(\kappa\kappa'-\kappa'^2)\tau}\sin\theta'\frac{\sin(w'\tau)}{w'}$$
$$\times\Big(\sin\theta'\cos\phi'$$
$$\times\left\{\hat{u}_1(\underline{\kappa}-\underline{\kappa}',0)+\hat{u}_3(\underline{\kappa}-\underline{\kappa}',0)\frac{1-\cos(w''\tau)}{w''^2}\frac{(\kappa_1-\kappa_1')(\kappa_3-\kappa_3')}{(\kappa-\kappa')^2}\right\} \quad (3.58)$$
$$+\sin\theta'\sin\phi'$$
$$\times\left\{\hat{u}_2(\underline{\kappa}-\underline{\kappa}',0)+\hat{u}_3(\underline{\kappa}-\underline{\kappa}',0)\frac{1-\cos(w''\tau)}{w''^2}\frac{(\kappa_2-\kappa_2')(\kappa_3-\kappa_3')}{(\kappa-\kappa')^2}\right\}$$
$$+\cos\theta'\hat{u}_3(\underline{\kappa}-\underline{\kappa}',0)\cos(w''\tau)\Big)d\kappa' d\theta' d\phi'.$$

Moving to the nonlinear term $\hat{M}$ which appears in the momentum equation, see (3.19), we expand the repeated indices to generate a total of 12 convolutions:

$$\hat{M}_j = i\frac{\kappa_j}{\kappa^2}\big[\kappa_1\hat{u}_1 * \kappa_1\hat{u}_1 + \kappa_2\hat{u}_1 * \kappa_1\hat{u}_2 + \kappa_3\hat{u}_1 * \kappa_1\hat{u}_3 +$$
$$\kappa_1\hat{u}_2 * \kappa_2\hat{u}_1 + \kappa_2\hat{u}_2 * \kappa_2\hat{u}_2 + \kappa_3\hat{u}_2 * \kappa_2\hat{u}_3 + \quad (3.59)$$
$$\kappa_1\hat{u}_3 * \kappa_3\hat{u}_1 + \kappa_2\hat{u}_3 * \kappa_3\hat{u}_2 + \kappa_3\hat{u}_3 * \kappa_3\hat{u}_3\big]$$
$$-i(\kappa_1\hat{u}_j * \hat{u}_1 + \kappa_2\hat{u}_j * \hat{u}_2 + \kappa_3\hat{u}_j * \hat{u}_3)$$

The expansion of the nine terms inside the square brackets are labeled by the row and column position $M_{(row,column)}$ and exclude the preceding quantity, $i\kappa_j/\kappa^2$. The expansion of the three terms inside the curved brackets, terms 10, 11, and 12, respectively, for j = 1, 2, and 3 are labeled by term and corresponding value of j. These expansions have been placed below similar terms from within the square brackets. Furthermore, square brackets have been placed to separate quantities that are similar among all terms.

$$M_{(1,1)} = e^{-Gr^{-1}\kappa^2\tau}\int_0^{2\pi}\int_0^{\pi}\int_0^{\infty}\hat{b}(\underline{\kappa},0)\hat{b}(\underline{\kappa}-\underline{\kappa}',0)\kappa'^3 e^{2Gr^{-1}(\kappa\kappa'-\kappa'^2)\tau}\left[\frac{\sin 2\theta'}{2}\sin\theta'\cos^2\phi\frac{(\kappa_1-\kappa_1')^2(\kappa_3-\kappa_3')}{(\kappa-\kappa')^2}\right]\frac{1}{w''}\sin(w'\tau)\sin(w''\tau)d\kappa' d\theta' d\phi' \quad (3.60)$$

$$M_{\left(\substack{10\\j=1}\right)} = e^{-Gr^{-1}\kappa^2\tau}\int_0^{2\pi}\int_0^{\pi}\int_0^{\infty}\hat{b}(\underline{\kappa},0)\hat{b}(\underline{\kappa}-\underline{\kappa}',0)\kappa'^3 e^{2Gr^{-1}(\kappa\kappa'-\kappa'^2)\tau}\left[\frac{\sin 2\theta'}{2}\sin\theta'\cos^2\phi\frac{(\kappa_1-\kappa_1')(\kappa_3-\kappa_3')}{(\kappa-\kappa')^2}\right]\frac{1}{w''}\sin(w'\tau)\sin(w''\tau)d\kappa' d\theta' d\phi' \quad (3.61)$$

$$M_{(1,2)} = e^{-Gr^{-1}\kappa^2\tau}\int_0^{2\pi}\int_0^{\pi}\int_0^{\infty}\hat{b}(\underline{\kappa},0)\hat{b}(\underline{\kappa}-\underline{\kappa}',0)\kappa'^3 e^{2Gr^{-1}(\kappa\kappa'-\kappa'^2)\tau}\left[\frac{\sin 2\theta'}{2}\frac{\sin 2\phi'}{2}\sin\theta'\frac{(\kappa_1-\kappa_1')(\kappa_2-\kappa_2')(\kappa_3-\kappa_3')}{(\kappa-\kappa')^2}\right] \quad (3.62)$$
$$\times\frac{1}{w''}\sin(w'\tau)\sin(w''\tau)d\kappa' d\theta' d\phi'$$

$$M_{\left(\substack{11\\j=1}\right)} = e^{-Gr^{-1}\kappa^2\tau}\int_0^{2\pi}\int_0^{\pi}\int_0^{\infty}\hat{b}(\underline{\kappa},0)\hat{b}(\underline{\kappa}-\underline{\kappa}',0)\kappa'^3 e^{2Gr^{-1}(\kappa\kappa'-\kappa'^2)\tau}\left[\frac{\sin 2\theta'}{2}\frac{\sin 2\phi'}{2}\sin\theta'\frac{(\kappa_2-\kappa_2')(\kappa_3-\kappa_3')}{(\kappa-\kappa')^2}\right]\frac{1}{w''}\sin(w'\tau)\sin(w''\tau)d\kappa' d\theta' d\phi' \quad (3.63)$$

$$M_{(1,3)} = e^{-Gr^{-1}\kappa^2\tau}\int_0^{2\pi}\int_0^{\pi}\int_0^{\infty}\hat{b}(\underline{\kappa},0)\hat{b}(\underline{\kappa}-\underline{\kappa}',0)\kappa'^3 e^{2Gr^{-1}(\kappa\kappa'-\kappa'^2)\tau}\left[-\frac{\sin 2\theta'}{2}\cos\theta'\cos\phi' w''^2(\kappa_1-\kappa_1')\right]\frac{1}{w''}\sin(w'\tau)\sin(w''\tau)d\kappa' d\theta' d\phi' \quad (3.64)$$

$$M_{\left(\substack{12\\j=1}\right)} = e^{-Gr^{-1}\kappa^2\tau}\int_0^{2\pi}\int_0^{\pi}\int_0^{\infty}\hat{b}(\underline{\kappa},0)\hat{b}(\underline{\kappa}-\underline{\kappa}',0)\kappa'^3 e^{2Gr^{-1}(\kappa\kappa'-\kappa'^2)\tau}\left[-\frac{\sin 2\theta'}{2}\cos\theta'\cos\phi' w''^2\right]\frac{1}{w''}\sin(w'\tau)\sin(w''\tau)d\kappa' d\theta' d\phi' \quad (3.65)$$

$$M_{(2,1)} = e^{-Gr^{-1}\kappa^2\tau}\int_0^{2\pi}\int_0^{\pi}\int_0^{\infty}\hat{b}(\underline{\kappa},0)\hat{b}(\underline{\kappa}-\underline{\kappa}',0)\kappa'^3 e^{2Gr^{-1}(\kappa\kappa'-\kappa'^2)\tau}\left[\frac{\sin 2\theta'}{2}\frac{\sin 2\phi'}{2}\sin\theta'\frac{(\kappa_1-\kappa_1')(\kappa_2-\kappa_2')(\kappa_3-\kappa_3')}{(\kappa-\kappa')^2}\right] \quad (3.66)$$
$$\times\frac{1}{w''}\sin(w'\tau)\sin(w''\tau)d\kappa' d\theta' d\phi'$$

$$M_{\binom{10}{j=2}} = e^{-Gr^{-1}\kappa^2\tau}\int_0^{2\pi}\int_0^{\pi}\int_0^{\infty}\hat{b}(\underline{\kappa},0)\hat{b}(\underline{\kappa}-\underline{\kappa}',0)\kappa'^3 e^{2Gr^{-1}(\kappa\kappa'-\kappa'^2)\tau}\left[\frac{\sin 2\theta'}{2}\frac{\sin 2\phi'}{2}\sin\theta'\frac{(\kappa_1-\kappa_1')(\kappa_3-\kappa_3')}{(\kappa-\kappa')^2}\right]\frac{1}{w''}\sin(w'\tau)\sin(w''\tau)d\kappa' d\theta' d\phi' \quad (3.67)$$

$$M_{(2,2)} = e^{-Gr^{-1}\kappa^2\tau}\int_0^{2\pi}\int_0^{\pi}\int_0^{\infty}\hat{b}(\underline{\kappa},0)\hat{b}(\underline{\kappa}-\underline{\kappa}',0)\kappa'^3 e^{2Gr^{-1}(\kappa\kappa'-\kappa'^2)\tau}\left[\frac{\sin 2\theta'}{2}\sin\theta'\sin^2\phi'\frac{(\kappa_2-\kappa_2')^2(\kappa_3-\kappa_3')}{(\kappa-\kappa')^2}\right]\frac{1}{w''}\sin(w'\tau)\sin(w''\tau)d\kappa' d\theta' d\phi' \quad (3.68)$$

$$M_{\binom{11}{j=2}} = e^{-Gr^{-1}\kappa^2\tau}\int_0^{2\pi}\int_0^{\pi}\int_0^{\infty}\hat{b}(\underline{\kappa},0)\hat{b}(\underline{\kappa}-\underline{\kappa}',0)\kappa'^3 e^{2Gr^{-1}(\kappa\kappa'-\kappa'^2)\tau}\left[\frac{\sin 2\theta'}{2}\sin\theta'\sin^2\phi\frac{(\kappa_2-\kappa_2')(\kappa_3-\kappa_3')}{(\kappa-\kappa')^2}\right]\frac{1}{w''}\sin(w'\tau)\sin(w''\tau)d\kappa' d\theta' d\phi' \quad (3.69)$$

$$M_{(2,3)} = e^{-Gr^{-1}\kappa^2\tau}\int_0^{2\pi}\int_0^{\pi}\int_0^{\infty}\hat{b}(\underline{\kappa},0)\hat{b}(\underline{\kappa}-\underline{\kappa}',0)\kappa'^3 e^{2Gr^{-1}(\kappa\kappa'-\kappa'^2)\tau}\left[-\frac{\sin 2\theta'}{2}\cos\theta'\sin\phi' w''^2(\kappa_2-\kappa_2')\right]\frac{1}{w''}\sin(w'\tau)\sin(w''\tau)d\kappa' d\theta' d\phi' \quad (3.70)$$

$$M_{\binom{12}{j=2}} = e^{-Gr^{-1}\kappa^2\tau}\int_0^{2\pi}\int_0^{\pi}\int_0^{\infty}\hat{b}(\underline{\kappa},0)\hat{b}(\underline{\kappa}-\underline{\kappa}',0)\kappa'^3 e^{2Gr^{-1}(\kappa\kappa'-\kappa'^2)\tau}\left[-\frac{\sin 2\theta'}{2}\cos\theta'\sin\phi' w''^2\right]\frac{1}{w''}\sin(w'\tau)\sin(w''\tau)d\kappa' d\theta' d\phi' \quad (3.71)$$

$$M_{(3,1)} = e^{-Gr^{-1}\kappa^2\tau}\int_0^{2\pi}\int_0^{\pi}\int_0^{\infty}\hat{b}(\underline{\kappa},0)\hat{b}(\underline{\kappa}-\underline{\kappa}',0)\kappa'^3 e^{2Gr^{-1}(\kappa\kappa'-\kappa'^2)\tau}\left[-\sin^3\theta'\cos\phi'\frac{(\kappa_1-\kappa_1')(\kappa_3-\kappa_3')^2}{(\kappa-\kappa')^2}\right]\frac{1}{w''}\sin(w'\tau)\sin(w''\tau)d\kappa' d\theta' d\phi' \quad (3.72)$$

$$M_{\binom{10}{j=3}} = e^{-Gr^{-1}\kappa^2\tau}\int_0^{2\pi}\int_0^{\pi}\int_0^{\infty}\hat{b}(\underline{\kappa},0)\hat{b}(\underline{\kappa}-\underline{\kappa}',0)\kappa'^3 e^{2Gr^{-1}(\kappa\kappa'-\kappa'^2)\tau}\left[-\sin^3\theta'\cos\phi'\frac{(\kappa_1-\kappa_1')(\kappa_3-\kappa_3')}{(\kappa-\kappa')^2}\right]\frac{1}{w''}\sin(w'\tau)\sin(w''\tau)d\kappa' d\theta' d\phi' \quad (3.73)$$

$$M_{(3,2)} = e^{-Gr^{-1}\kappa^2\tau}\int_0^{2\pi}\int_0^{\pi}\int_0^{\infty}\hat{b}(\underline{\kappa},0)\hat{b}(\underline{\kappa}-\underline{\kappa}',0)\kappa'^3 e^{2Gr^{-1}(\kappa\kappa'-\kappa'^2)\tau}\left[-\sin^3\theta'\sin\phi'\frac{(\kappa_2-\kappa_2')(\kappa_3-\kappa_3')^2}{(\kappa-\kappa')^2}\right]\frac{1}{w''}\sin(w'\tau)\sin(w''\tau)d\kappa' d\theta' d\phi' \quad (3.74)$$

$$M_{\binom{11}{j=3}} = e^{-Gr^{-1}\kappa^2\tau}\int_0^{2\pi}\int_0^{\pi}\int_0^{\infty}\hat{b}(\underline{\kappa},0)\hat{b}(\underline{\kappa}-\underline{\kappa}',0)\kappa'^3 e^{2Gr^{-1}(\kappa\kappa'-\kappa'^2)\tau}\left[-\sin^3\theta'\sin\phi'\frac{(\kappa_2-\kappa_2')(\kappa_3-\kappa_3')}{(\kappa-\kappa')^2}\right]\frac{1}{w''}\sin(w'\tau)\sin(w''\tau)d\kappa' d\theta' d\phi' \quad (3.75)$$

$$M_{(3,3)} = e^{-Gr^{-1}\kappa^2\tau} \int_0^{2\pi}\int_0^{\pi}\int_0^{\infty} \hat{b}(\underline{\kappa},0)\hat{b}(\underline{\kappa}-\underline{\kappa}',0)\kappa'^3 e^{2Gr^{-1}(\kappa\kappa'-\kappa'^2)\tau} \left[\frac{\sin 2\theta'}{2}\sin\theta' w''^2\left(\kappa_3-\kappa_3'\right)\right]\frac{1}{w''}\sin(w'\tau)\sin(w''\tau)d\kappa' d\theta' d\phi' \quad (3.76)$$

$$M_{\left(\substack{12\\ j=1}\right)} = e^{-Gr^{-1}\kappa^2\tau} \int_0^{2\pi}\int_0^{\pi}\int_0^{\infty} \hat{b}(\underline{\kappa},0)\hat{b}(\underline{\kappa}-\underline{\kappa}',0)\kappa'^3 e^{2Gr^{-1}(\kappa\kappa'-\kappa'^2)\tau} \left[\frac{\sin 2\theta'}{2}\sin\theta' w''^2\right]\frac{1}{w''}\sin(w'\tau)\sin(w''\tau)d\kappa' d\theta' d\phi' \quad (3.77)$$

The nonlinear terms, $\hat{B}$ and $\hat{M}$, must be evaluated before the expressions can be inserted into (3.17) and (3.18). The ϕ' integral, including the group of $(\kappa_m - \kappa'_m)$ terms where wavenumber vector components from (3.9) have been inserted, can be solved directly and results in an expression dependent on θ' and κ'. For example, the first term inside the parentheses of (3.57) is:

$$\begin{aligned}
&\int_0^{2\pi} \cos\phi' \frac{(\kappa_1 - \kappa'_1)(\kappa_3 - \kappa'_3)}{(\kappa - \kappa')^2} d\phi' \\
&\quad = \int_0^{2\pi} \cos\phi' \frac{(\kappa\cos\phi\sin\theta - \kappa'\cos\phi'\sin\theta')(\kappa\cos\theta - \kappa'\cos\theta')}{(\kappa - \kappa')^2} d\phi' \\
&\quad = \frac{(\kappa\cos\theta - \kappa'\cos\theta')}{(\kappa - \kappa')^2} \int_0^{2\pi} \cos\phi'(\kappa\cos\phi\sin\theta - \kappa'\cos\phi'\sin\theta') d\phi' \\
&\quad = -\pi\kappa'\sin\theta' \frac{(\kappa\cos\theta - \kappa'\cos\theta')}{(\kappa - \kappa')^2}
\end{aligned} \tag{3.78}$$

A similar result is found for the second term inside the parentheses of (3.57) since the evaluation of $\cos^2\phi'$ and $\sin^2\phi'$ from 0 to 2π are equivalent.

Using the method of stationary phase to evaluate the asymptotic behavior of the θ' integral as $\tau \to \infty$, it is expected that the nonlinear terms will hold a form similar to

$$I(\tau) = \int_0^{\pi} F(\theta') e^{i\tau G(\theta')} d\theta' \approx F(\theta_S) \sqrt{\frac{2\pi}{\tau |G''(\theta_S)|}} e^{i\tau G(\theta_S) + i(\pi/4)\mathrm{sgn}[G''(\theta_S)]} \tag{3.79}$$

where $\theta' = \theta_S$ represents the stationary point (i.e., $G'(\theta') = 0$), F and G are functions determined when forming the integrand from $\hat{B}$ and $\hat{M}$, and the signum function (sgn) determines the sign of the exponential phase component (e.g., $\pi/4$). Long-time behavior is of interest here because that is when nonlinear interactions are likely to influence the turbulence (Hanazaki and Hunt, 1996). The rationale behind the method of stationary phase is that contributions to the integral primarily come from the end points or from a 'flat' region near the stationary point of a function. Oscillations of the $G(\theta')$ function that occur between each of the end points and the stationary point will cancel out of the integral. KH also evaluated the asymptotic behavior for the nonlinear terms for strained flow, but the integrals were of a different form.

The κ' integral, which involves various combinations of the initial velocity and buoyancy fields and convolution terms involving κ and κ', must be also be solved in order to complete the evaluation of the nonlinear terms. Initial conditions for isotropic turbulence will be generated using an approach similar to Rogallo (1981) where the initial conditions for the Fourier velocity are defined as:

$$\hat{u}_{10} = \frac{(\chi\kappa\kappa_2 + \psi\kappa_1\kappa_3)}{\kappa(\kappa_1^2 + \kappa_2^2)^{1/2}}\ , \tag{3.80}$$

$$\hat{u}_{20} = \frac{(\psi\kappa_2\kappa_3 - \chi\kappa\kappa_1)}{\kappa(\kappa_1^2 + \kappa_2^2)^{1/2}}\ , \tag{3.81}$$

$$\hat{u}_{30} = -\frac{\psi(\kappa_1^2 + \kappa_2^2)^{1/2}}{\kappa}\ , \tag{3.82}$$

and

$$\chi = \left(\frac{E(k)}{4\pi\kappa^2}\right)^{1/2} e^{i\gamma_1}\cos\Omega\,, \tag{3.83}$$

$$\psi = \left(\frac{E(k)}{4\pi\kappa^2}\right)^{1/2} e^{i\gamma_2}\sin\Omega\,. \tag{3.84}$$

The specified energy spectrum function $E(k)$ is shown in (2.9), γ_1 and γ_2 are the spatial phase distribution and Ω is the velocity component distribution. The distributions consist of random numbers between 0 and 2π (Rogallo, 1981).

Preliminary investigations to understand the influence of nonlinear terms were completed by numerically solving a model problem. The model system is representative of the form we anticipate to see once the nonlinear integrals are solved.[16] The two model ordinary differential equations solved are

$$\frac{dW}{dt} = -A^2B - PW + M^*\mathrm{E}t^{-1/2}\sin(Ct+\xi)e^{-Rt} \tag{3.85}$$

$$\frac{dB}{dt} = W - QB - B^*\mathrm{E}t^{-1/2}\sin(Ct+\xi)e^{-Rt} \tag{3.86}$$

where these equations hold the same general form as (3.17) and (3.18), W and B represent the Fourier coefficients, and A, P and Q are coefficients related to the time scale, Grashof

[16] Matlab code developed for model problem is found in Appendix A.

number, and Schmidt number. The last term in each equation is the expected form of $\hat{B}$ and $\hat{M}$ where the parameters M^*, B^*, E, C, R, and ξ result from the nonlinear term approximation.

Solving the set of ordinary differential equations in (3.85) and (3.86) for W and B, a comparison between extended and original (i.e., nonlinear terms neglected) RDT model equations can be made (Figure 3.5). Model operation was verified by evaluating a special case (e.g., $E = 0$) to ensure that predictions of the Fourier coefficients using the extended model agree with original RDT when no nonlinear terms were present (Figure 3.5a). The model values of $P = 0.1$ and $Q = 0.01$ correspond to $Gr \approx 10$ and $Sc \approx 10$, respectively. The influence of the nonlinear terms on the Fourier coefficient behavior is immediately seen through the introduction of arbitrary values for the nonlinear term parameters (Figure 3.5b). Further adjustment of the nonlinear terms through M^* and B^*, the relative frequency C, or the phase ξ results in amplitude and period changes to the Fourier coefficient curves (Figure 3.5c and Figure 3.5d). The signs present in front of the nonlinear terms also influence the behavior; when both signs are negative the curves shift to the left and the amplitude increases. However, when both signs are positive an increase in amplitude is still observed but the curves shift to the right. The +/- or -/+ combination in front of the nonlinear terms present in (3.85) and (3.86) resulted in significant amplitude changes, but no shift in the timing. Even though these variations in W and B do not provide a direct relationship to changes that may be seen in vertical flux correlation coefficient curves, it does imply that the addition of expressions for nonlinear terms has the ability to increase the decay of the Fourier coefficients, a prominent feature of moderately stratified flows seen in Figure 3.3. The presence of nonlinear terms also influences the turbulent parameter timing, specifically an increase in the period is observed.

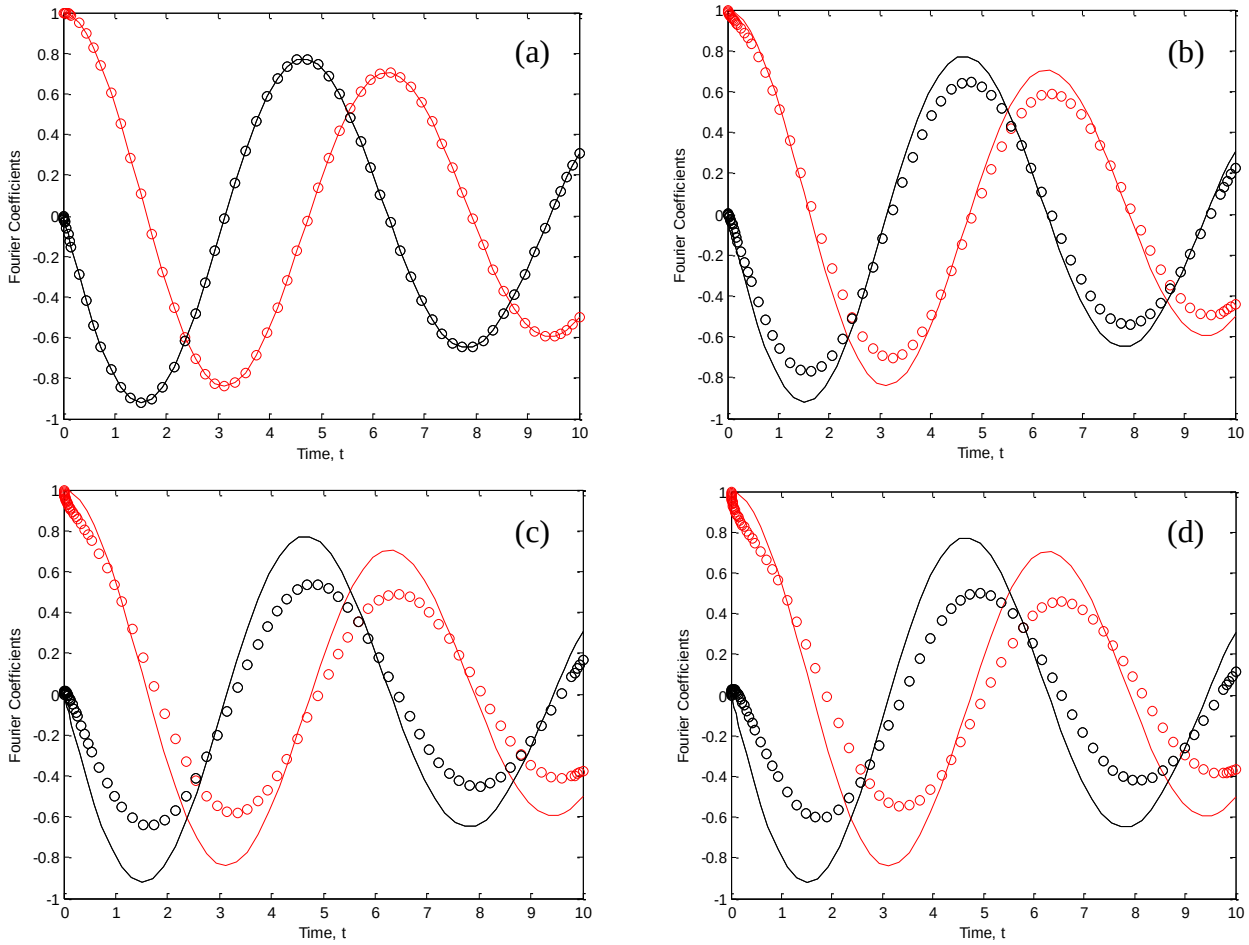

Figure 3.5: Comparison of Fourier coefficient behavior between extended RDT (○ = *W* and ○ = *B*) and original RDT (— = *W* and — = *B*) with various parameter changes for $A = 0.1$, $P = 0.1$ and $Q = 0.01$: (a) $E = 0$, curves match; (b) $M^* = B^* = 1$, $E = 0.1$, $C = R = 1$, $\xi = \pi/4$; (c) $M^* = B^* = 2$, $E = 0.1$, $C = 0.5$, $\xi = \pi/4$, $R = 1$; (d) $M^* = B^* = 2$, $E = 0.1$, $C = 0.5$, $\xi = \pi/2$, $R = 1$.[17]

[17] Matlab code used to generate figure: RDTExModel.m

Conclusions

Several attempts at modifying RDT from its original form to were made to better reflect moderately stratified flows. None of the initial attempts of RDT parameter modification, simulations, or extensions using other turbulence models were able to predict the peak timing or magnitude of the vertical flux at large times, which is when nonlinear interactions are expected to be more relevant in stratified flows. However, there are inherent challenges, although more mathematical in nature, of incorporating nonlinear terms into the governing RDT equations using an approach similar to KH.

Evaluation of the model RDT equations implies that the addition of some form of a nonlinear term to each of the differential equations has the ability to influence the timing and magnitude of the fluxes. However, more insight into the exact form of the nonlinear term integrals is necessary. The stationary points would need to be determined for each of the different θ' integrals and method of stationary phase applied. Special care will need to be taken when imaginary numbers are present, as the stationary points may differ or contribution to the integral may come from other sources. The approach by Rogallo (1981) will need to be applied to generate initial conditions for the velocity field. In addition, an expression for the initial density field $\hat{b}_0$ will need to be developed so that Rogallo's approach can be applied. This should then result in one integrand, combined with the results from the stationary phase approximation, to be evaluated in terms of κ'.

Once the nonlinear term integrals are evaluated, the $O(Fr)$ ordinary differential equations can be solved analytically to get Fourier coefficients, $\hat{u}_3^{(1)}$ and $\hat{b}^{(1)}$. From there, the cospectrum of vertical velocity and buoyancy can be constructed using the definition provided by Hanazaki and Hunt (1996):

$$E_{b3}(\boldsymbol{\kappa},t) = \tfrac{1}{2}\left(\overline{\hat{b}\hat{u}_3^*} + \overline{\hat{b}^*\hat{u}_3}\right) \tag{3.87}$$

where $\hat{b} = \hat{b}^{(0)} + Fr\hat{b}^{(1)}$ and $\hat{u}_3 = \hat{u}_3^{(0)} + Fr\hat{u}_3^{(1)}$. The spectrum can then be integrated over all wavespace to obtain the fluxes and plotted at a function of time. Similarly, the extended RDT equations could also be solved numerically by developing differential equations and initial

conditions for the spectra and then integrated to get fluxes. Results can be compared to the DNS results by Gerz and Yamazaki (1993), and the experimental results by LVA and YW.

Extension of RDT through the addition of the normally neglected nonlinear terms will work to increase the applicability of this turbulence model to flows commonly seen in the environment. Nonlinear interactions influence the behavior of turbulent flows in terms of the amount of mass transferred and when restratification will occur. While other approaches are used to incorporate nonlinear interactions, such as the simpler eddy viscosity model to the more complicated stochastic modeling approaches, development of an analytical solution is desired for investigating behaviors and ease of use.

CHAPTER 4: GENERAL CONCLUSIONS

Summary

Understanding the behavior of turbulence in stratified flows is necessary for evaluation of the mixing and transport that occurs in lakes, oceans, and other geophysical flows. Rapid distortion theory (RDT) was used to obtain analytical expressions for vertical fluxes that were then used to determine the mixing efficiency for cases of one and two active scalars. The mixing efficiency η varied as a function of the Grashof number Gr, which measures the importance of buoyancy and viscosity, the Schmidt number Sc, which varies over three orders of magnitude from heated air to saltwater, and the density ratio R_ρ, which compares the density changed caused by temperature and the density change caused by salinity in the case of two active scalars.

Nonlinear interactions can potentially influence not only the mixing efficiency, but also the behavior of turbulence in general. Nonlinear interactions are accounted for in turbulence models in various ways or neglected, as in standard RDT. An approach similar to Kevlahan and Hunt (1997) was used to develop quantitative expressions for the nonlinear terms neglected from RDT. Predictions from a model system based on the expected asymptotic form of the nonlinear terms show that these terms do influence turbulence behavior.

Significant Findings

The research pertaining to mixing efficiency evaluation and extension of RDT to more moderately stratified flows resulted in several important contributions:

- An analytical solution for the vertical density flux was derived for the two scalar case of salt and heat.
- Results for the one scalar case show that when Gr is large, η decreases as Sc increases and that the mixing efficiency increases with Gr up to a maximum value, as in laboratory experiments and numerical simulations.
- The maximum mixing efficiency of approximately 30% for low Sc is consistent with values from simulations, and the maximum efficiency of 6% for heated water is

consistent with laboratory measurements. However, RDT underpredicts the maximum efficiency for saltwater and the value of *Gr* at which the efficiency decreases.

- For two active scalars, RDT predicts similar behavior as that for one scalar, and the efficiency decreases as R_ρ decreases.
- Initial attempts to extend RDT to moderately stratified flows through parameter modification, simulations, or extensions using other turbulence models were not able to predict the peak timing or lack of upgradient flux at large times as observed in experiments. Parameter modification could predict the approximate magnitude and timing of either the first or second peak of the correlation curve, but not both simultaneously. Simulations primarily affected the magnitude of correlation coefficient with minimal impact to peak timing.
- Expressions for the nonlinear terms typically neglected from RDT governing equations were derived using an approach similar to Kevlahan and Hunt (1997).
- A model system including the addition of the expected form of the nonlinear terms was developed to gain insight into how nonlinear interactions influence the period and decay of turbulence parameters.

Future Work

Further research includes evaluation of the integrals present in the nonlinear terms added on to the governing RDT equations. Explicit nonlinear expressions should then replace the expected form used in the model system. The updated system of equations could then be solved both analytically, similar to the approach used in Chapter 3, or numerically. Once the system of equations is solved, fluxes could be compared to simulations (Gerz and Yamazaki, 1993) and experiments (Lienhard and Van Atta, 1990; Yoon and Warhaft, 1990). Comparing the fluxes generated using the extended and original RDT models could provide further insight into the vortex mode and timing of when nonlinear effects are seen. Additional investigations could be made to further increase the applicability of the extended RDT model: for example, to flows with $Sc \neq 1$, flows where initial velocity and buoyancy fields are present, or to inhomogeneous turbulence. Furthermore, fluxes computed using the extended RDT model could be used to determine the mixing efficiency.

APPENDIX A: MATLAB FUNCTIONS

This research required extensive use of MATLAB to compute results presented in Chapter 2. Below are the codes to compute and evaluate mixing efficiencies and the produce the corresponding figures.

RDT – One Active Scalar Case

```
% File name: RFlux.m
% Purpose: Compute the Richardson Flux number analytically using Hanazaki
% and Hunt (1996) equation for vertical density flux (Eqn. 4.22, Page
% 314)and solving the time integration analytically.

% Date Created: 11.9.12
% Date Modified: 3.2.13

function Rf = func_RFlux(Gri,Sc)

%  Set constants
r = 0;            % r = peke = 3*eta0

ntheta   = 100;
thetamin = 0.0001;
thetamax = pi;
theta    = linspace(thetamin,thetamax,ntheta);

nk  = 400;
k   = linspace(0.0001,14,nk);

[K,THETA] = meshgrid(k,theta);

% Energy spectrum function
Ek  = (K.^4.*exp(-K.^2/2))/(3*(2*pi)^(1/2));

% Equation for mixing efficiency
g   = 0.5*((1-2*r*Sc)/(1+Sc))*...
      (Ek.*(sin(THETA)).^3)./((sin(THETA)).^2+(K.^4.*Gri^2)/Sc);

% Numerical integration of equation for mixing efficiency
Rf  = trapz(k,(trapz(theta,g)));
```

```
% File name: Rfdriver.m

% Clean up
clear; close all

% Set conditions
Sc    = [0.1 0.5 1 2]';
%Sc   = [0.1 0.5 1 3 7 10 20 50 100 200 700]';
```

```
nSc   = length(Sc);

Gri   = logspace(-5,1);
%Gri  = [0.1 0.01 0.001 0.0001];
nGri  = length(Gri);

Rf = NaN*ones(nGri,nSc);

for i = 1:nGri
    for j = 1:nSc
        Rf(i,j) = func_RFlux(Gri(i),Sc(j));
    end
end
```

RDT – Two Active Scalar Case

```
% File name: DDFlux.m
% Purpose: Compute the Richardson Flux number analytically for the two
% active scalar case (i.e., differential diffusion).

% Date Created: 1.11.13

function Rf = func_DDFlux(Gri, Rrho)

% Set conditions
ScT         = 7;
ScS         = 700;

ntheta      = 30;     %Number of points to discretize theta
thetamin    = 0;
thetamax    = pi;
dtheta      = (thetamax)/(ntheta-1);
theta       = thetamin:dtheta:thetamax;

nk      = 20;     %Number of points to discretize k
kmin    = 0.001;
kmax    = 10;
k       = linspace(kmin,kmax,nk);

% Analytical solution for cubic roots, DLMF Section 1.11
[THETA,K] = meshgrid(theta,k);

a  = Gri*K.^2;
aT = Gri*(ScT)^(-1)*K.^2;
aS = Gri*(ScS)^(-1)*K.^2;
b  = sin(THETA).^2;
gT = -Rrho/(1+Rrho);
gS = 1/(1+Rrho);

z3 = 1;
z2 = a + aT + aS;
z1 = a.*aT + a.*aS + aT.*aS + b;
z0 = a.*aS.*aT-(aS*gT - aT*gS).*b;

p  = (3*z1-z2.^2)./3;
q  = (2*z2.^3-9*z2.*z1+27*z0)./27;

D1 = -4*p.^3-27*q.^2;

A  = ((-27/2)*q+(3/2)*sqrt(-3*D1)).^(1/3);
B  = -(3*p)./A;

rho = (-1/2)+(1/2)*sqrt(-3);

%These 3 sigma values are the eigenvalues for system of u3, uT, uS eqns.
sig1 = (1/3)*(A+B)-(1/3)*z2;
sig2 = (1/3)*(rho*A+rho^2*B)-(1/3)*z2;
```

```
sig3 = (1/3)*(rho^2*A+rho*B)-(1/3)*z2;

% Information for eigenvectors (A1, A2, A3, B1, B2, B3, C1, C2, C3)
GT = repmat(gT,nk,ntheta);
GS = repmat(gS,nk,ntheta);

f1 = GT./(sig1+aT);        g1 = GS./(sig1+aS);
f2 = GT./(sig2+aT);        g2 = GS./(sig2+aS);
f3 = GT./(sig3+aT);        g3 = GS./(sig3+aS);

a33 = (f1.*g2-f2.*g1)./(f1.*g2-f1.*g3-f2.*g1+f2.*g3+f3.*g1-f3.*g2);
a3T = (g1-g2)./(f1.*g2-f1.*g3-f2.*g1+f2.*g3+f3.*g1-f3.*g2);
a3S = -(f1-f2)./(f1.*g2-f1.*g3-f2.*g1+f2.*g3+f3.*g1-f3.*g2);
a23 = (-f1-(f3-f1).*a33)./(f2-f1);
a2T = (1-(f3-f1).*a3T)./(f2-f1);
a2S = ((f1-f3).*a3S)./(f2-f1);
a13 = 1-a23-a33;
a1T = -a2T-a3T;
a1S = -a2S-a3S;

b33 = f3.*a33;
b3T = f3.*a3T;
b3S = f3.*a3S;
b23 = f2.*a23;
b2T = f2.*a2T;
b2S = f2.*a2S;
b13 = f1.*a13;
b1T = f1.*a1T;
b1S = f1.*a1S;

c33 = g3.*a33;
c3T = g3.*a3T;
c3S = g3.*a3S;
c23 = g2.*a23;
c2T = g2.*a2T;
c2S = g2.*a2S;
c13 = g1.*a13;
c1T = g1.*a1T;
c1S = g1.*a1S;

% Initial conditions
E330 = (K.^2.*exp(-0.5*K.^2).*(sin(THETA)).^2)/(12*pi*sqrt(2*pi));

% Equations for spectra - assuming no initial temperature or salinity
% fluctuations
s1c1 = sig1+conj(sig1);
s1c2 = sig1+conj(sig2);
s1c3 = sig1+conj(sig3);
s2c1 = sig2+conj(sig1);
s2c2 = sig2+conj(sig2);
s2c3 = sig2+conj(sig3);
s3c1 = sig3+conj(sig1);
s3c2 = sig3+conj(sig2);
s3c3 = sig3+conj(sig3);
```

```
% Plot flux as a function of time
nt     = 100;                % Number of times to report the values
tend   = 10*pi;              % End time of the simulation
dt     = tend/(nt-1);        % Time increment (dimensionless)
tspans = 0:dt:tend;          % Time span (dimensionless)

FT3 = NaN*ones(nt,1);
FS3 = NaN*ones(nt,1);

for it = 1:nt
    tspan = tspans(it);
ET3 = 0.5*E330.*((a13.*conj(b13)+conj(a13).*b13).*exp(s1c1.*tspan)+...
                 (a13.*conj(b23)+conj(a23).*b13).*exp(s1c2.*tspan)+...
                 (a13.*conj(b33)+conj(a33).*b13).*exp(s1c3.*tspan)+...
                 (a23.*conj(b13)+conj(a13).*b23).*exp(s2c1.*tspan)+...
                 (a23.*conj(b23)+conj(a23).*b23).*exp(s2c2.*tspan)+...
                 (a23.*conj(b33)+conj(a33).*b23).*exp(s2c3.*tspan)+...
                 (a33.*conj(b13)+conj(a13).*b33).*exp(s3c1.*tspan)+...
                 (a33.*conj(b23)+conj(a23).*b33).*exp(s3c2.*tspan)+...
                 (a33.*conj(b33)+conj(a33).*b33).*exp(s3c3.*tspan));

ES3 = 0.5*E330.*((a13.*conj(c13)+conj(a13).*c13).*exp(s1c1.*tspan)+...
                 (a13.*conj(c23)+conj(a23).*c13).*exp(s1c2.*tspan)+...
                 (a13.*conj(c33)+conj(a33).*c13).*exp(s1c3.*tspan)+...
                 (a23.*conj(c13)+conj(a13).*c23).*exp(s2c1.*tspan)+...
                 (a23.*conj(c23)+conj(a23).*c23).*exp(s2c2.*tspan)+...
                 (a23.*conj(c33)+conj(a33).*c23).*exp(s2c3.*tspan)+...
                 (a33.*conj(c13)+conj(a13).*c33).*exp(s3c1.*tspan)+...
                 (a33.*conj(c23)+conj(a23).*c33).*exp(s3c2.*tspan)+...
                 (a33.*conj(c33)+conj(a33).*c33).*exp(s3c3.*tspan));

FT3(it) = 2*pi*squeeze(trapz(theta, trapz(k, ET3.*K.^2).*sin(theta)));
FS3(it) = 2*pi*squeeze(trapz(theta, trapz(k, ES3.*K.^2).*sin(theta)));

end

% Integrate spectra analytically with respect to time
TET3 = 0.5*E330.*((a13.*conj(b13)+conj(a13).*b13).*(-1./s1c1)+...
                  (a13.*conj(b23)+conj(a23).*b13).*(-1./s1c2)+...
                  (a13.*conj(b33)+conj(a33).*b13).*(-1./s1c3)+...
                  (a23.*conj(b13)+conj(a13).*b23).*(-1./s2c1)+...
                  (a23.*conj(b23)+conj(a23).*b23).*(-1./s2c2)+...
                  (a23.*conj(b33)+conj(a33).*b23).*(-1./s2c3)+...
                  (a33.*conj(b13)+conj(a13).*b33).*(-1./s3c1)+...
                  (a33.*conj(b23)+conj(a23).*b33).*(-1./s3c2)+...
                  (a33.*conj(b33)+conj(a33).*b33).*(-1./s3c3));

TES3 = 0.5*E330.*((a13.*conj(c13)+conj(a13).*c13).*(-1./s1c1)+...
                  (a13.*conj(c23)+conj(a23).*c13).*(-1./s1c2)+...
                  (a13.*conj(c33)+conj(a33).*c13).*(-1./s1c3)+...
                  (a23.*conj(c13)+conj(a13).*c23).*(-1./s2c1)+...
                  (a23.*conj(c23)+conj(a23).*c23).*(-1./s2c2)+...
                  (a23.*conj(c33)+conj(a33).*c23).*(-1./s2c3)+...
```

```
                (a33.*conj(c13)+conj(a13).*c33).*(-1./s3c1)+...
                (a33.*conj(c23)+conj(a23).*c33).*(-1./s3c2)+...
                (a33.*conj(c33)+conj(a33).*c33).*(-1./s3c3));

% Integrate k and theta numerically
FT = 2*pi*squeeze(trapz(theta, trapz(k, TET3.*K.^2).*sin(theta)));
FS = 2*pi*squeeze(trapz(theta, trapz(k, TES3.*K.^2).*sin(theta)));

%Compute mixing efficiency
Rf = 2*(FS - FT);
```

```
% DDFluxdriver

% Clean up
clear; close all

% Set conditions
Rrho   = [0.001 0.01 0.1 1]';
nRrho  = length(Rrho);

Gri    = logspace(-5,1);
%Gri   = [10 5 3 2 1 0.9 0.7 0.5 0.3 0.1 0.05 0.01 0.001 0.0001];
nGri   = length(Gri);

Rf = NaN*ones(nGri,nRrho);

for i = 1:nGri
    for j = 1:nRrho
        Rf(i,j) = func_DDFlux(Gri(i),Rrho(j));
    end
end
```

Extended RDT Model System

```
% File name: RDTExModel.m
% Purpose: Solve system of RDT differential equations numerically with
% expected form of nonlinear terms included.

% Date created: 3.31.13

% Clean up
clear; close all

% Set parameters
a = 2;
p = 1;
q = 1;
c = 1;
r = 1;
ep = 0.1;      %For special case, set ep=0, then 'standard' and 'extended'
               cases match
M1 = 4;
B1 = 4;
x = pi/4;      %Phase

b0 = 1;

% Set constants
tend   = 6;              %  End time of the simulation
w0     = [0,b0];         %  Initial conditions

% Solve the ODE
[t,w]  = ode45('RDTExModelEqn',[0.001 tend],w0,[],a,p,ep,M1,c,r,q,B1,x);

% Plot w and b

% Original RDT is the 'standard' RDT where nonlinear terms are not
% considered, see Equationsystem.m.
load RDTOrig

figure (1);hold on
plot(t,w(:,1),'k',t,w(:,2),'r')
plot(t0,w0(:,1),'ko',t0,w0(:,2),'ro')      %Compare to 'standard' RDT
xlabel('Time, t')
ylabel('Fourier Coeffient')
box on
```

```
function dw= RDTExModelEqn( t,w,flag,a,p,ep,M1,c,r,q,B1,x)

dw(1)=-a^2*w(2)-p*w(1)+t^(-1/2)*ep*M1*cos(c*t+x)*exp(-r*t);
dw(2)=w(1)-q*w(2)-t^(-1/2)*ep*B1*cos(c*t+x)*exp(-r*t);
dw=dw';

end
```

APPENDIX B: MODEL EXTENSION ATTEMPTS

Explanations of the different extension attempts and figures comparing the attempted models and experimental data as part of the initial investigations are presented here.

Modification of RDT Input Parameters

There are three dimensionless inputs to rapid distortion theory (RDT): the Grashof number *Gr*, Schmidt number *Sc*, and the initial ratio of potential and kinetic energy *r*. The Grashof number is the ratio of buoyant to viscous forces and can be expressed in a variety of forms

$$Gr = \frac{NL^2}{\nu} = \frac{Re}{Fr} = ReRi^{1/2} \tag{B.1}$$

where *N* is the buoyancy frequency, *L* is proportional to the longitudinal integral length scale, and *v* is the kinematic viscosity. The other dimensionless parameters include the Reynolds number *Re*, the Froude number *Fr*, and the Richardson number *Ri*. The Schmidt number describes the ratio of kinematic viscosity to molecular diffusivity of a fluid: for example, *Sc* = 0.7 for heated air, 7 for heated water, and 700 for saltwater.

The first, most basic, attempt to better replicate moderately stratified conditions using RDT was done through iterations of *Gr* and *r* combinations. Selection of the input values was based on observed parameter behavior (Figure B.1 and Figure B.2). For a constant value of *r*, as *Gr* increases the vertical flux correlation coefficient curve shifts upward with the most significant vertical differences seen at early times (Figure B.1a). For larger *Gr* the turbulence decays faster (Figure B.1b) likely due to the increased kinematic viscosity (i.e., faster diffusion of momentum).

For constant *Gr*, the amplitude decreases as *r* increases (Figure B.2a). Similar to Figure B.1a, the vertical flux correlation coefficient correlation curves dampen as time progresses as a result of decaying turbulence. The initial density fluctuations must sort themselves out through restratification. When the flow is fully turbulent at $r = 0$, the flux is initially downgradient, but as it increases the restratification reduces the downgradient flux to a point that it is eventually upgradient. Changes to the vertical fluxes are shown in Figure B.2b.

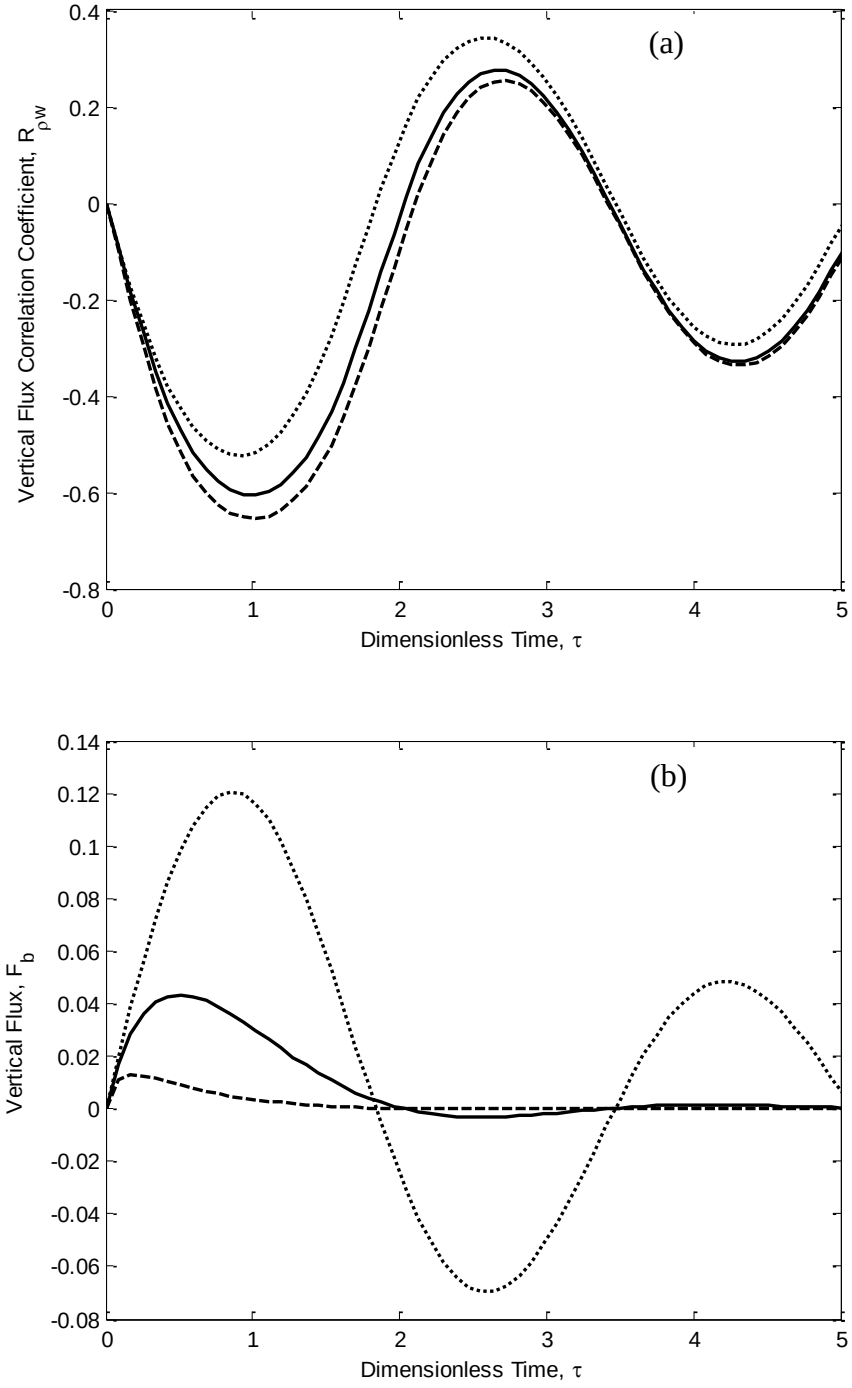

Figure B.1: Comparison of (a)[18] vertical flux correlation coefficient curves and (b)[19] vertical flux curves for varying *Gr*: *Gr* = 0.01 (···), *Gr* = 0.2 (—), and *Gr* = 1 (— —) for *r* = 1.35 and *Sc* = 0.7.

[18] Matlab code used to generate figure: compare_plot_1.m
[19] Matlab code used to generate figure: compare_plot_2.m

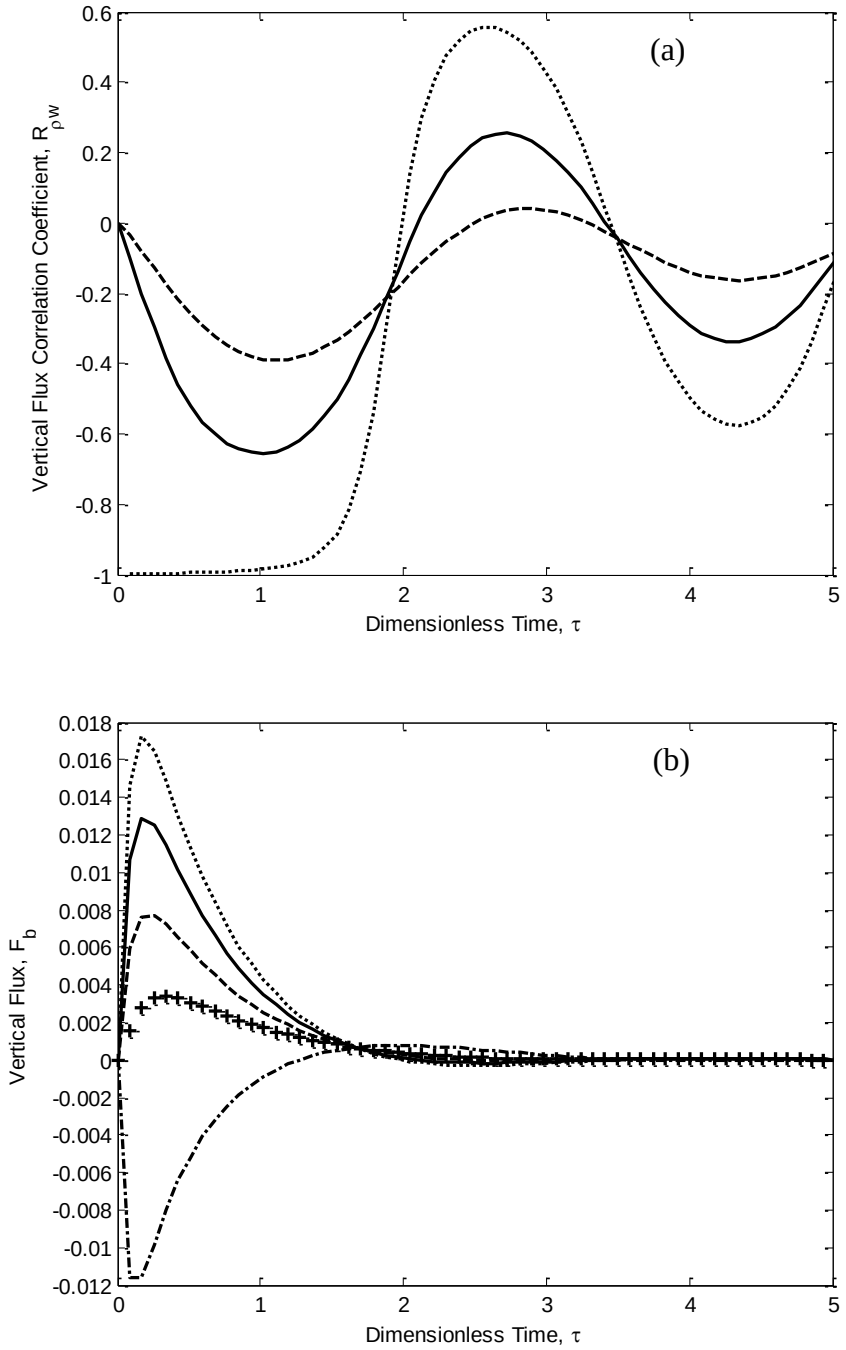

Figure B.2: Comparison of (a)[20] vertical flux correlation coefficient curves and (b)[21] vertical flux curves for varying energy ratios: r = 0 (···), r = 1.35 (—), r = 3 (— —), r = 4.5 (+), and r = 9 (–●–) for Gr = 1.25 and Sc = 0.7.

[20] Matlab code used to generate figure: compare_plot_3.m
[21] Matlab code used to generate figure: compare_plot_4.m

None of the *Gr* and *r* combinations input to RDT were able to predict the peak timing and magnitude of the experimental data (Figure B.3). The various combinations could either match the first or second peak of the experimental data, but not both simultaneously. This could indicate that the turbulent parameter responsible for the behavior change depends on time.

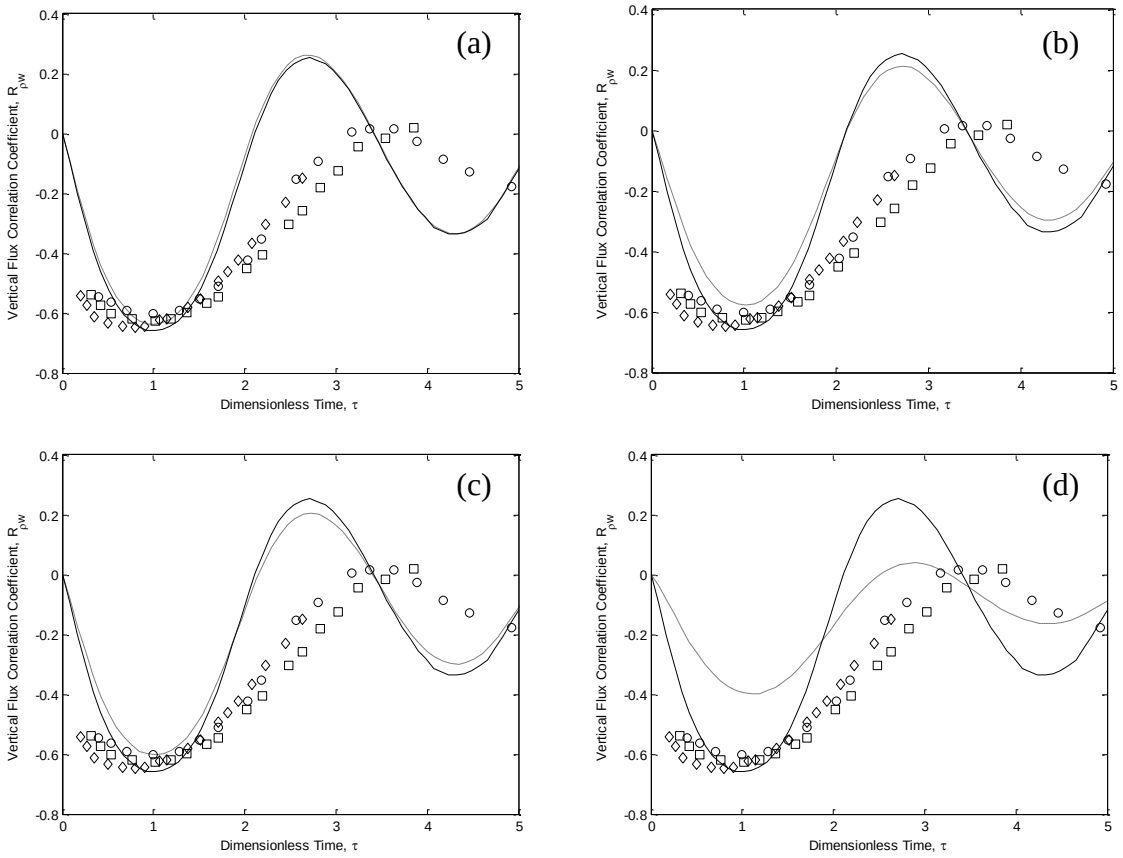

Figure B.3: Comparison of LVA (○, *Fr* = 17.1; □, *Fr* = 21.8; ◊, *Fr* = 32.4) experiments, RDT (–, *Gr* = 1 and *r* = 1.35), and RDT with modified parameters (···) (a) *Gr* = 2.25 and *r* = 1.35; (b) *Gr* = 2.25 and *r* = 1.65; (c) *Gr* = 1 and *r* = 1.65; (d) *Gr* = 1and *r* = 3 at *Sc* = 0.7.[22]

[22] Matlab code used to generate figure: lva.m

Varying Turbulent Diffusivity

Nonlinear interactions represented through a turbulent eddy diffusivity was incorporated into RDT where its value was recalculated at each time step of the numerical model allowing it to change as a function of time. The turbulent eddy diffusivity D_T used here is defined as

$$D_T = \frac{-flux}{gradient} = \frac{\frac{g}{T}\left(-\overline{u_3 T'}\right)}{\frac{dT}{dx_3}} \tag{B.2}$$

and can be computed at each time step using Lienhard and Van Atta (1990) data for N = 2.42 s^{-1} (their Table 1).Variables in the turbulent diffusivity definition include the acceleration due to gravity g, temperature T, vertical velocity u_3 in the vertical direction x_3, and fluctuating temperature T'. The turbulent diffusivity decreases over time (Figure B.4) and can be represented by:

$$D_T = -2.41\times10^{-7}t^3 + 3.48\times10^{-6}t^2 - 1.58\times10^{-5}t + 2.3\times10^{-5}. \tag{B.3}$$

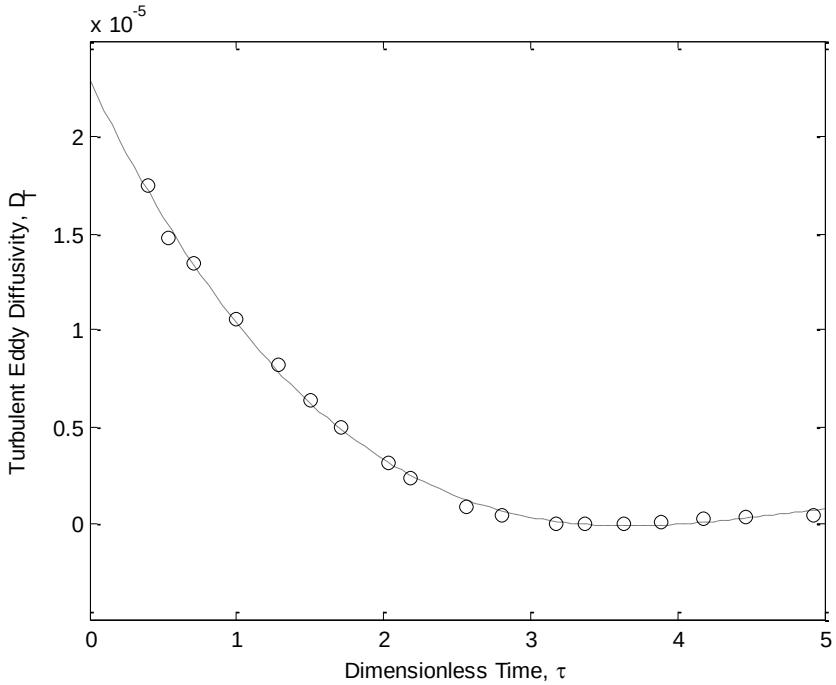

Figure B.4: Relationship between turbulent diffusivity and time: ○, LVA data and **--,** best fit line.[23]

[23] MATLAB code used to produce figure: FigB4.m

The diffusivity relationship in (B.3) is unique to this particular data set and was used to redefine the *Gr* and *Sc* inputs to the numerical RDT model. As a result, *N* and the length scale *L* must be specified. The length scale for use in the numerical model can be determined using longitudinal integral length scale information from Yoon and Warhaft (1990) in combination with Lienhard and Van Atta (1990) data. The integral length scale using velocity fluctuations in the horizontal direction L_u provided in Yoon and Warhaft (1990) is calculated as:

$$\frac{L_u}{M} = \frac{\frac{(u_1)^3}{\varepsilon}}{M} = \frac{\frac{(0.1678\,m/s)^3}{0.373\,m^2/s^3}}{0.0508m} = 0.25 \qquad \text{(B.4)}$$

where u_1 is the root mean square horizontal velocity and ε is the energy dissipation at measuring station A** for mesh size *M* (see Lienhard and Van Atta (1990) Table 1). The length scale ratio in (B.4) corresponds to a distance ratio downstream of the grid *x/M* of approximately 5 (see Yoon and Warhaft (1990) Figure 7b) which in turn corresponds to a longitudinal integral scale L_f ratio (L_f/M) of approximately 0.25 (per Yoon and Warhaft (1990) notation, see Figure 7a). For a mesh size of 0.0508 m, L_f = 0.0127 m. Substituting this value into the length scale and longitudinal integral scale relationship, the length scale for use in the numerical model is

$$L = \left(\frac{\pi}{2}\right)^{-1/2} \ell = \left(\frac{\pi}{2}\right)^{-1/2} 0.0127\text{m} = 0.01\text{m} \ . \qquad \text{(B.5)}$$

Use of a varying diffusivity in the RDT model moves the correlation curve vertically, but still does not reflect the experimental data at long times (Figure B.5). The diffusivity relationship (B.3) was also multiplied by a range of scaling factors and no better alignment was achieved. The same eddy diffusivity relationship is applied to all spectra and it could be possible that the eddy diffusivity varies over both wavenumber space and time.

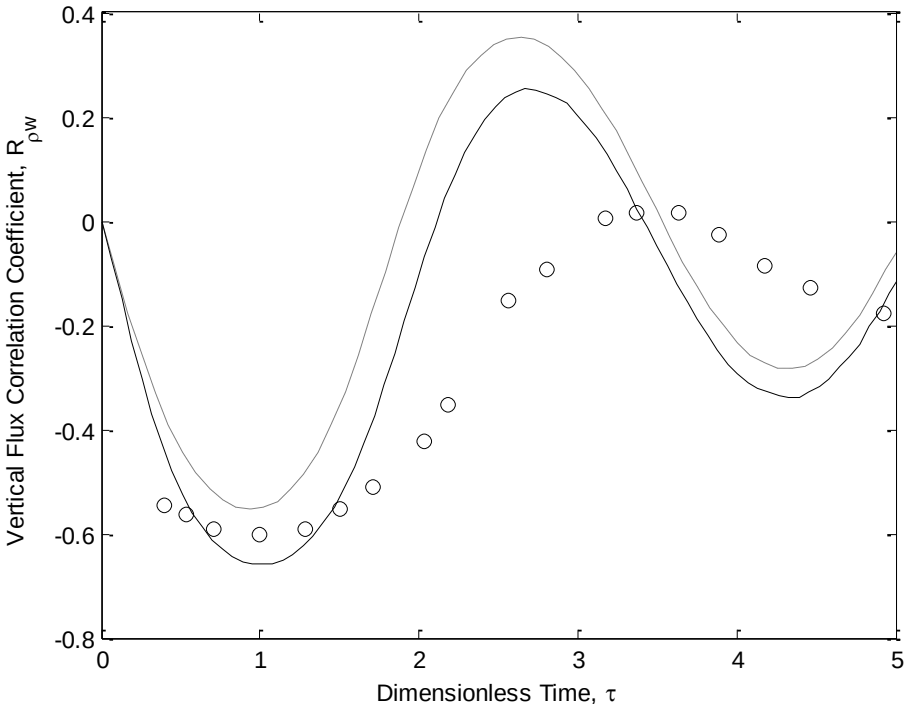

Figure B.5: Comparison of vertical flux correlation curves using RDT with constant diffusivity (—, Gr = 1 and r = 1.35), RDT with varying diffusivity (···, Gr = 1, r = 1.35, N = 2.42 rad/s and L = 0.01m), and LVA experiments (○, Fr = 17.1 and N = 2.42 rad/s) for Sc = 0.7.[24]

[24] MATLAB code used to produce figure: varD.m

Diffusivity Simulation

In an attempt to reflect variations in D_T that may be due to the wavenumber k and time t, a new vertical density flux was computed for each time step and then used to calculate a new D_T. Figure B.6 shows the overall concept of this approach.

The general definition of D_T used for this simulation is similar to (B.2), but computation of the vertical density flux R_{34} is computed numerically based on the spectra given inputs of Gr, Sc, N, ℓ and TKE:

$$D_T = \frac{-flux}{gradient} = \frac{-\overline{\rho' u_3'}}{\frac{\partial \rho}{\partial x_3}} = \frac{-\frac{g}{\rho_0}\left(\overline{\rho' u_3'}\right)}{\frac{\partial}{\partial x_3}\left(\frac{g}{\rho_0}\bar{\rho}\right)} = \frac{\text{TKE}}{4}\frac{R_{34}}{N} \tag{B.6}$$

where ρ_0, $\bar{\rho}$, and ρ' are the reference, background, and fluctuating densities, respectively, and TKE can be computed directly from Lienhard and Van Atta (1990) data.

Results using the above approach are shown in Figure B.7. Unfortunately, output more closely matches the original RDT solution and Lienhard and Van Atta (1990) data. Near $\tau \approx 3$ the diffusivity simulation was unable to meet integration tolerances (i.e., the abrupt termination of the correlation curve). This numerical error was not explored further since the solution does not appear to reflect the experimental data.

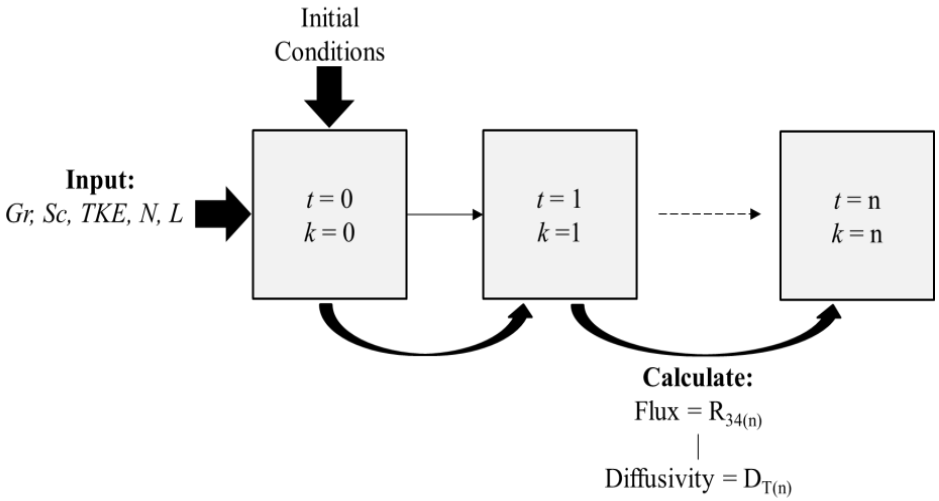

Figure B.6: Flowchart showing overall strategy for turbulent diffusivity simulation model.[25]

[25] Figure location: RDT Flow Chart.pptx

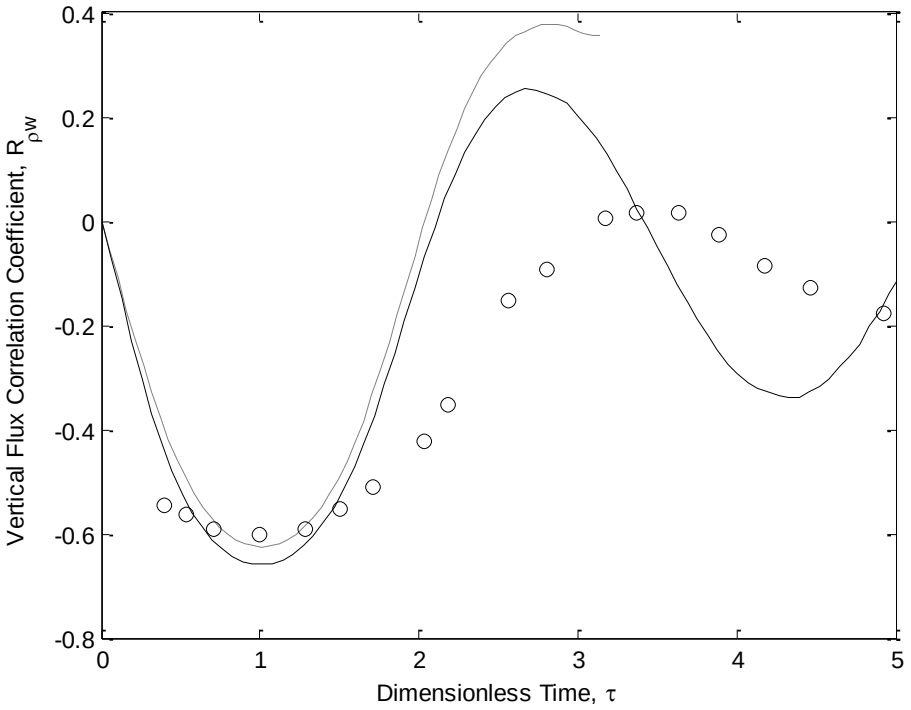

Figure B.7: Comparison of vertical flux correlation curves using RDT with constant diffusivity (—, Gr = 1 and r = 1.35), RDT simulation with varying diffusivity (···,Gr = 1, r = 1.35, L = 0.01m and TKE = 0.04 m^2/s^2), and LVA experiment (○, Fr = 17.1 and N = 2.42 rad/s) for Sc = 0.7.[26]

[26] MATLAB code used to produce figure: DTsim.m

k-*ε* Model

Since the varying diffusivity and diffusivity simulation did not improve the ability of RDT to reflect the experimental data, an approach using the *k*-*ε* model was tried. For this turbulence model, the velocity and length components of the turbulent eddy viscosity ν_t are solved for through two quantities: *k* (meaning turbulent kinetic energy in this application, not wavenumber) and the rate of dissipation of turbulent kinetic energy, ε. Transport equations for each quantity are developed and solved instead of just simply specifying the term ν_t as in eddy viscosity models. The *k*-equation for steady flow can be written as

$$U\frac{dk}{dx} = \frac{g}{\rho_0}\frac{\nu_t}{\sigma_t}\frac{\partial\bar{\rho}}{\partial z} - \varepsilon \tag{B.7}$$

where $\sigma_t = 1$ is a specified coefficient, $\partial\bar{\rho}/\partial x_3$ is the background density gradient, and both energy generation and divergence of turbulent flux terms have been neglected (Rodi, 1987). The ε-equation for steady flow can be written as

$$U\frac{d\varepsilon}{dx} = -c_{1\varepsilon}c_{3\varepsilon}\frac{N^2 c_\mu k}{\sigma_t} - c_{2\varepsilon}\frac{\varepsilon^2}{k} \tag{B.8}$$

where $c_{1\varepsilon} = 1.44$, $c_{2\varepsilon} = 1.92$, and $c_{3\varepsilon} = 0.2$ are specified coefficients and c_μ is the proportionality coefficient (Rodi, 1987). The divergence of dissipative flux and one of the energy generation terms are neglected from (B.8). The terms on the right side of represent the other energy generation term and a destruction term, respectively.

Lienhard and Van Atta (1990) provide ample data for comparison to the *k*-*ε* model, whereas Yoon and Warhaft (1990) do not. Initial conditions for *k* and ε were taken to be at the first measuring station (i.e., Lienhard and Van Atta (1990) location A**) for the case of $N = 2.42$ rad/s and $M = 5.08$ centimeter (see Lienhard and Van Atta (1990) Table 1). Figure B.8 shows a comparison of the numerical model and experimental data. It can be observed that the flux decays over time and that the magnitude range is similar for both curves, but the *k*-ε model does not accurately represent the trend of the measured data points. The observation of decreasing flux values makes physical sense because at early times both horizontal and vertical velocities will be large, but as time increase the vertical velocity becomes smaller (as the turbulence decays) and the horizontal velocity dominates.

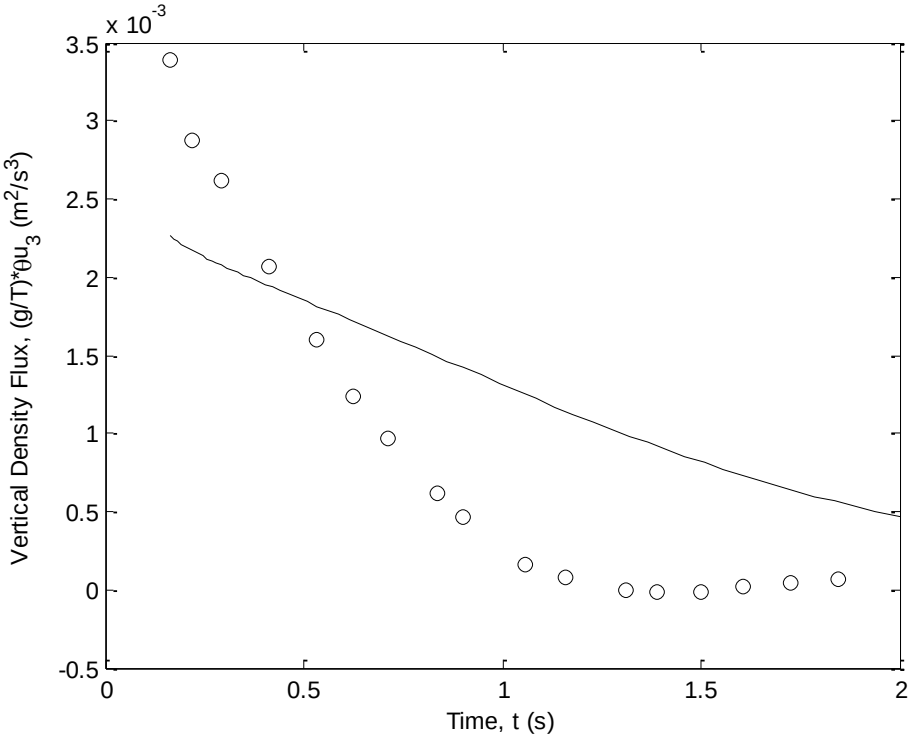

Figure B.8: Comparison of vertical density flux using the *k*-ε model numerical solution (—) and LVA experiment (○, *Fr* = 17.1 and *N* = 2.42 rad/s).[27]

[27] MATLAB code used to produce figures: ke.m

Diffusivity Simulation with *k*-ε model

Combining the strategy from the previous two attempts, a simulation is performed using an eddy viscosity similar to that for the *k*-ε model, where the viscosity is determined by multiplying a length scale and a velocity scale. This approach works to avoid the production of negative diffusivity values. Similar to the previous diffusivity simulation model, initial conditions and inputs must be specified. For each time step, new fluxes are calculated along with an energy spectra, length scale, and velocity scale where the eddy viscosity and diffusivity can then be determined for each wavenumber *k* and time step. Pardon the notation overlap between the wavenumber and the standard turbulent kinetic energy symbol in the *k*-ε model. Figure B.9 shows the overall concept of this approach.

The length scale L_3 is represented by the longitudinal length scale in the vertical direction

$$L_3 = \frac{\pi E_3(0)}{2\overline{u_3' u_3'}} = \frac{\pi E_3(0)}{2R_{33}} \tag{B.9}$$

where E_3 is the one dimensional energy spectra at time equal to zero and R_{33} vertical velocity flux (Pope, 2000). The one dimensional energy spectra is represented by

$$E_3 = 2\sin\theta \iint E_{33} k \, dk d\phi \tag{B.10}$$

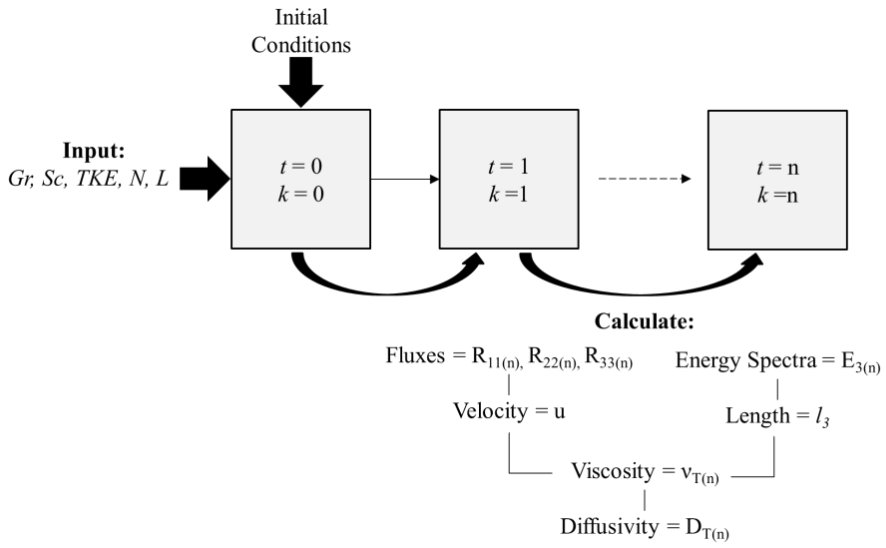

Figure B.9: Flowchart showing overall strategy for turbulent diffusivity simulation model using *k*-ε model approach.[28]

[28] Figure location: RDT Flow Chart.pptx

where E_{33} is the three dimensional energy spectra. Substitution of (B.10) into (B.9) yields the length scale component for the eddy viscosity. The velocity scale can be obtained by taking the square root of the turbulent kinetic energy

$$u_0 = \sqrt{R_{11} + R_{22} + R_{33}} \tag{B.11}$$

where R_{11} and R_{22} are velocity fluxes in the corresponding directions. The length scale is then multiplied by the velocity scale to obtain the eddy viscosity and ultimately the turbulent diffusivity. Output using the above approach is shown in Figure B.10. Again, this output more closely matches the original RDT results and still does not reflect Lienhard and Van Atta (1990) data. It must be noted that this particular simulation model does not have a time limitation, unlike the first diffusivity simulation attempt.

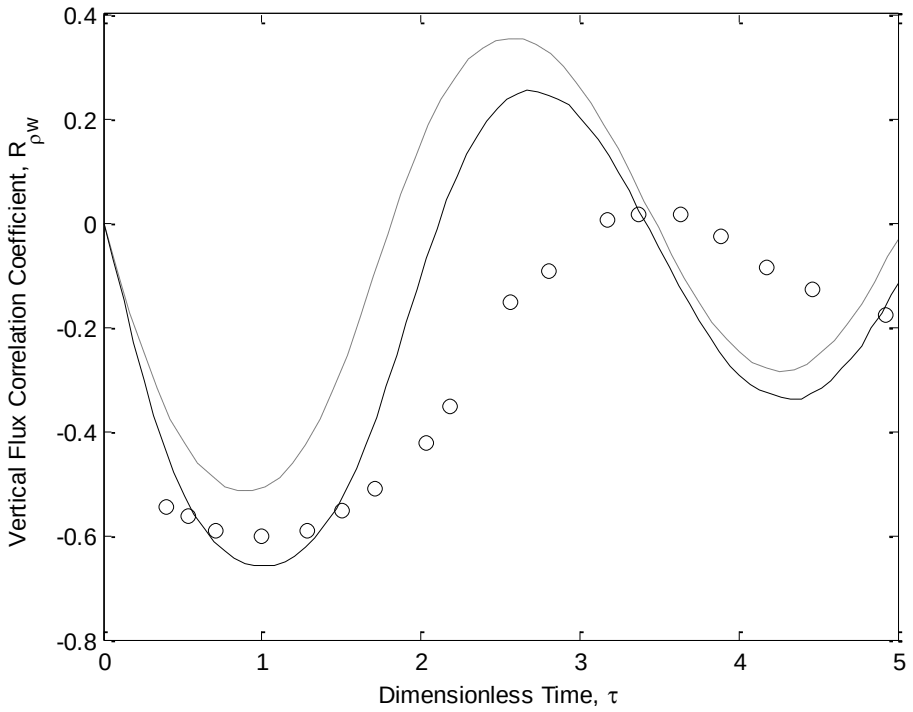

Figure B.10: Comparison of vertical flux correlation curves using RDT with constant diffusivity (—, Gr = 1 and r = 1.35), RDT simulation with varying diffusivity based on k-ε model approach (···,Gr = 1, r = 1.35, L = 0.01m and TKE = 0.04 m^2/s^2), and LVA experiment (○, Fr = 17.1 and N=2.42 rad/s) for Sc = 0.7.[29]

[29] MATLAB code used to produce figure: DTsimke.m

REFERENCES

Ayyalasomayajula, S. and Warhaft, Z., 2006. Nonlinear interactions in strained axisymmetric high-Reynolds-number turbulence. Journal of Fluid Mechanics, 566: 273-307.

Barrett, T.K. and Van Atta, C.W., 1991. Experiments on the inhibition of mixing in stably stratified decaying turbulence using laser Doppler anemometry and laser-induced fluorescence. Physics of Fluids, A3(5): 1321-1332.

Brethouwer, G., Hunt, J.C.R. and Nieuwstadt, F.T.M., 2003. Micro-structure and Lagrangian statistics of the scalar field with a mean gradient in isotropic turbulence. Journal of Fluid Mechanics, 474: 193-225.

Britter, R.E., 1985. Diffusion and decay in stably-stratified turbulent flows, Hunt, J.C.R. (Ed.), Turbulence and Diffusion in Stable Environments, Claredon, Oxford, pp. 3-13.

Cambon, C., Mansour, N.N. and Godeferd, F.S., 1997. Energy transfer in rotating turbulence. Journal of Fluid Mechanics, 337: 303-332.

Cambon, C. and Scott, J.F., 1999. Linear and nonlinear models of anisotropic turbulence. Annual Review of Fluid Mechanics, 31: 1-53.

Elsinga, G.E. and Marusic, I., 2010. Universal aspects of small-scale motions in turbulence. Journal of Fluid Mechanics, 662: 514-539.

Etemad-Shahidi, A. and Imberger, J., 2002. Anatomy of turbulence in a narrow and strongly stratified estuary. Journal of Geophysical Research-Oceans, 107(C7).

Fernando, H.J.S., 1991. Turbulent mixing in stratified fluids. Annual Review of Fluid Mechanics, 23: 455-493.

Ferrari, R. and Polzin, K.L., 2005. Finescale structure of the T-S relation in the eastern North Atlantic. Journal of Physical Oceanography, 35(8): 1437-1454.

Frisch, U., 1995. Turbulence: The Legacy of A.N. Kolmogorov. Cambridge University Press, 296 pp.

Galmiche, M. and Hunt, J.C.R., 2002. The formation of shear and density layers in stably stratified turbulent flows: linear processes. Journal of Fluid Mechanics, 455: 243-262.

Gargett, A.E., Merryfield, W.J. and Holloway, G., 2003. Direct numerical simulation of differential scalar diffusion in three-dimensional stratified turbulence. Journal of Physical Oceanography, 33(8): 1758-1782.

Gargett, A.E. and Moum, J.N., 1995. Mixing efficiencies in turbulent tidal fronts - results from direct and indirect measurements of density flux. Journal of Physical Oceanography, 25(11): 2583-2608.

Gargett, A.E., Osborn, T.R. and Nasmyth, P.W., 1984. Local isotropy and the decay of turbulence in a stratified fluid. Journal of Fluid Mechanics, 144(JUL): 231-280.

Gerz, T. and Yamazaki, H., 1993. Direct numerical-simulation of buoyancy-driven turbulence in stably stratified fluid. Journal of Fluid Mechanics, 249: 415-440.

Godeferd, F.S., Cambon, C. and Scott, J.F., 2001. Two-point closures and their applications: report on a workshop. Journal of Fluid Mechanics, 436: 393-407.

Gotoh, T., Rogallo, R.S., Herring, J.R. and Kraichnan, R.H., 1993. Lagrangian velocity correlations in homogeneous isotropic turbulence. Physics of Fluids A, 5(11): 2846-2864.

Graebel, W.P., 2007. Advanced Fluid Mechanics. Academic Press.

Gregg, M.C., 1987. Diapycnal Mixing in the Thermocline: A Review. Journal of Geophysical Research, 92(C5): 5249-5286.

Hanazaki, H. and Hunt, J.C.R., 1996. Linear processes in unsteady stably stratified turbulence. Journal of Fluid Mechanics, 318: 303-337.

Hanazaki, H. and Hunt, J.C.R., 2004. Structure of unsteady stably stratified turbulence with mean shear. Journal of Fluid Mechanics, 507: 1-42.

Herring, J.R. and Kerr, R.M., 1993. Development of enstrophy and spectra in numerical turbulence. Physics of Fluids A-Fluid Dynamics, 5(11): 2792-2798.

Hunt, J.C.R., Sandham, N.D., Vassilicos, J.C., Launder, B.E., Monkewitz, P.A. and Hewitt, G.F., 2001. Developments in turbulence research: a review based on the 1999 Programme of the Isaac Newton Institute , Cambridge. Journal of Fluid Mechanics, 436: 353-391.

Imberger, J. and Ivey, G.N., 1991. On the Nature of Turbulence in a Stratified Fluid. Part II: Application to Lakes. Journal of Physical Oceanography, 21(5): 659-680.

Isaza, J.C. and Collins, L.R., 2009. On the asymptotic behaviour of large-scale turbulence in homogeneous shear flow. Journal of Fluid Mechanics, 637: 213-239.

Ivey, G.N. and Imberger, J., 1991. On the Nature of Turbulence in a Stratified Fluid. Part I: The Energetics of Mixing. Journal of Physical Oceanography, 21(5): 650-658.

Jackson, P.R. and Rehmann, C.R., 2003a. Kinematic effects of differential transport on mixing efficiency in a diffusively stable, turbulent flow. Journal of Physical Oceanography, 33(1): 299-304.

Jackson, P.R. and Rehmann, C.R., 2003b. Laboratory measurements of differential diffusion in a diffusively stable, turbulent flow. Journal of Physical Oceanography, 33(8): 1592-1603.

Jackson, P.R. and Rehmann, C.R., 2009. Theory for differential transport of scalars in sheared stratified turbulence. Journal of Fluid Mechanics, 621: 1-21.

Jackson, P.R., Rehmann, C.R., Saenz, J.A. and Hanazaki, H., 2005. Rapid distortion theory for differential diffusion. Geophysical Research Letters, 32(10).

Kevlahan, N.K.R. and Hunt, J.C.R., 1997. Nonlinear interactions in turbulence with strong irrotational straining. Journal of Fluid Mechanics, 337: 333-364.

Kraichnan, R.H., 1991. Turbulent cascade and intermittency growth, Hunt, J.C.R., O.M. Phillips, D. Williams (Ed.),Turbulence and Stochastic Processes. The Royal Society.

Kundu, P.K. and Cohen, I.M., 2008. Fluid Mechanics. Elsevier Inc.

Liechtenstein, L., Godeferd, F.S. and Cambon, C., 2005. Nonlinear formation of structures in rotating stratified turbulence. Journal of Turbulence, 6(24).

Lienhard, J.H. and Van Atta, C.W., 1990. The decay of turbulence in thermally stratified flow. Journal of Fluid Mechanics, 210: 57-112.

Martin, J.E. and Rehmann, C.R., 2006. Layering in a flow with diffusively stable temperature and salinity stratification. Journal of Physical Oceanography, 36(7): 1457-1470.

Mellor, G.L. and Yamada, T., 1982. Development of a turbulence-closure model for geophysical and fluid problems. Reviews of Geophysics, 20(4): 851-875.

Moum, J.N., 1997. Quantifying vertical fluxes from turbulence in the ocean. Oceanography, 10(3): 111-115.

Nash, J.D. and Moum, J.N., 2002. Microstructure estimates of turbulent salinity flux and the dissipation spectrum of salinity. Journal of Physical Oceanography, 32(8): 2312-2333.

NIST, 2012. Digital Library of Mathematical Functions.

Osborn, T.R., 1980. Estimates of the local rate of vertical diffusion from dissipation measurements. Journal of Physical Oceanography, 10: 83-89.

Pope, S.B., 2000. Turbulent flows. Cambridge University Press, Cambridge ; New York, 771 pp.

Ravens, T.M., Kocsis, O., Wuest, A. and Granin, N., 2000. Small-scale turbulence and vertical mixing in Lake Baikal. Limnology and Oceanography, 45(1): 159-173.

Rehmann, C.R. and Koseff, J.R., 2004. Mean potential energy change in stratified grid turbulence. Dynamics of Atmospheres and Oceans, 37(4): 271-294.

Riley, J.J. and Lelong, M.P., 2000. Fluid motions in the presence of strong stable stratification. Annual Review of Fluid Mechanics, 32: 613-657.

Rodi, W., 1987. Examples of calculation methods for flow and mixing in stratified fluids. Journal of Geophysical Research-Oceans, 92(C5): 5305-5328.

Rogallo, R.S., 1981. Numerical experiments in homogeneous turbulence. NASA Technical Memorandum 81315. NASA, Ames Research Center.

Rottman, J.W. and Britter, R.E., 1986. The mixing efficiency and decay of grid-generated turbulence in stably stratified fluids, 9th Australasian Fluid Mechanics Conference, University of Auckland, December 8-12, 1986. Auckland, New Zealand.

Saggio, A. and Imberger, J., 2001. Mixing and turbulent fluxes in the metallimnion of a stratified lake. Limnology and Oceanography, 46(2): 392-409.

Smyth, W.D., Nash, J.D. and Moum, J.N., 2005. Differential diffusion in breaking Kelvin-Helmholtz billows. Journal of Physical Oceanography, 35(6): 1004-1022.

Stacey, M.T., Monismith, S.G. and Burau, J.R., 1999. Observations of turbulence in a partially stratified estuary. Journal of Physical Oceanography, 29(8): 1950-1970.

Stevens, C.L., 2003. Turbulence in an estuarine embayment: Observations from Beatrix Bay, New Zealand. Journal of Geophysical Research-Oceans, 108(C2).

Stretch, D.D., Rottman, J.W., Venayagamoorthy, S.K., Nomura, K.K. and Rehmann, C.R., 2010. Mixing efficiency in decaying stably stratified turbulence. Dynamics of Atmospheres and Oceans, 49(1): 25-36.

Teixeira, M.A.C., 2011. A linear model for the structure of turbulence beneath surface water waves. Ocean Modelling, 36(1-2): 149-162.

Tennekes, H. and Lumley, J.L., 1972. A first course in turbulence. MIT Press, Cambridge, Massachusetts, 300 pp.

Turner, J.S., 1973. Buoyancy Effects in Fluids. Cambridge University Press.

Wuest, A., van Senden, D.C., Imberger, J., Piepke, G. and Gloor, M., 1996. Comparison of diapycnal diffusivity measured by tracer and microstructure techniques. Dynamics of Atmospheres and Oceans, 24(1-4): 27-39.

Yoon, K.H. and Warhaft, Z., 1990. The evolution of grid-generated turbulence under conditions of stable thermal stratification. Journal of Fluid Mechanics, 215: 601-638.